Advancements in nanoscratch technology and its applications in cement-based materials A review

He, Zhi hai; Zhai, Wen qiang; Shi, Jin yan; Du, Cheng; Sun, Ruo miao; Yalçınkaya, Çağlar; Šavija, Branko

DOI
10.1016/j.pmatsci.2025.101435

Publication date
2025

Document Version
Final published version

Published in
Progress in Materials Science

Citation (APA)
He, Z. H., Zhai, W. Q., Shi, J. Y., Du, C., Sun, R. M., Yalçınkaya, Ç., & Šavija, B. (2025). Advancements in nanoscratch technology and its applications in cement-based materials: A review. *Progress in Materials Science*, *151*, Article 101435. https://doi.org/10.1016/j.pmatsci.2025.101435

Progress in Materials Science 151 (2025) 101435

Contents lists available at ScienceDirect

Progress in Materials Science

journal homepage: www.elsevier.com/locate/pmatsci

Advancements in nanoscratch technology and its applications in cement-based materials: A review

Zhi-hai He [a,b], Wen-qiang Zhai [a], Jin-yan Shi [c,*], Cheng Du [d], Ruo-miao Sun [a], Çağlar Yalçınkaya [e], Branko Šavija [f]

[a] College of Civil Engineering, Shaoxing University, Shaoxing 312000 China
[b] Key Laboratory of Rock Mechanics and Geohazards of Zhejiang Province, Shaoxing 312000 China
[c] School of Materials Science and Engineering, Southeast University, Nanjing 211189 China
[d] Service Department of Industry-College Cooperation, Beijing Institute of Economics and Management, Beijing 100102 China
[e] Department of Civil Engineering, Faculty of Engineering, Dokuz Eylül University, İzmir, Turkiye
[f] Faculty of Civil Engineering and Geosciences, Delft University of Technology, Delft, The Netherlands

ARTICLE INFO

Keywords:
Cement-based materials
Nanoscale features
Nanoscratch
Microstructure
Nanomechanical properties

ABSTRACT

Cement-based materials (CBMs) are multiscale composites whose macroscopic properties largely depend on their micro/nanoscale features. Micro and nanomechanical properties of CBMs are typically characterized using local techniques such as nanoindentation. Compared with nanoindentation, the nanoscratch allows for continuous measurement of CBMs to acquire more comprehensive and reliable nanomechanical information, which has provided a powerful tool for the characterization of CBMs at nanoscale. However, previous reviews on the application of nanoscratch in CBMs are relatively scarce and lack detailed guidance regarding specimen preparation methods and the testing procedure. This review presents a detailed discussion of specimen preparation procedures and requirements, measurements, and data analysis methods for nanoscratch testing applied to CBMs. Then, the nanomechanical properties derived from nanoscratch tests, including hardness, friction coefficient, elastic recovery ratio and fracture properties, have been summarized and discussed. Furthermore, the current uses of nanoscratch technique in CBMs, including characterization of nanoscale micorstructure, interface, tribological features, and fracture properties, are elaborated. On the nanoscale, the nanomechanical properties are employed for phase identification and to obtain the corresponding volume fractions. In addition, nanoscratch is widely utilized to identify the width, hardness, and fracture toughness of the interfacial transition zones, and to distinguish the interface between unreacted phases and hydration products. The combination of nanoscratch and other advanced techniques, such as atomic force microscopy, backscattered electron imaging, and acoustic emission to characterize the nanoscale micorstructures of CBMs is further discussed, which contributes to improving the accuracy of nanoscratch test results and broadens their applicability. In addition, some perspectives on testing methods, data analysis, and multifunctional applications of nanoindentation technology are proposed. This review aims to assist researchers in developing robust and reliable protocols for nanoscratch testing, thereby advancing the deeper understanding of the nanoscale features of CBMs.

* Corresponding author.
E-mail address: jinyan.shi@csu.edu.cn (J.-y. Shi).

https://doi.org/10.1016/j.pmatsci.2025.101435
Received 30 June 2024; Received in revised form 27 October 2024; Accepted 18 January 2025
Available online 21 January 2025

Acronyms

A_{LB}	Contact area
A_P	Vertical area projection
A(d)	Projected contact area
AFM	Atomic force microscopy
ASR	Alkali-silica reaction
BSE	Backscattered electron
CA	Coarse aggregate
C-A-S-H	Calcium-alumina −silicate-hydrate
CBMs	Cement-based materials
CDF	Cumulative distribution function
CF	Carbon fiber
CH	Calcium hydroxide
CL	Constant loading
CNF	Carbon nanofiber
COF	Coefficient of friction
DCL	Displacement-controlled loading
EDS	Energy dispersive spectroscopy
ERR	Elastic recovery ratio
FA	Fly ash
FCL	Force-controlled loading
F_{eq}	Equivalent force
FNA	Fine aggregate
F_T	Transverse force
F_V	Vertical force
GNP	Graphene nanoparticles
GO	Graphene oxide
HD-CSH	High-density gel phase
H/E	Hardness to elastic modulus
h_i	Penetration depth
H_{max}	Maximum scratch depth
HPC	High-performance concrete
H_P	Ploughing hardness
hr	Residual scratch depth
H_S	Ordinary scratch hardness
HX	Helical carbon nanotubes
ITZ	Interfacial transition zone
IS	Iron sheet
K_C	Fracture toughness
LD-CSH	Low-density gel phase
LEFM	Linear elastic fracture mechanics
LIL	Linearly increasing loading
MWCNT	Multi-walled carbon nanotube
OPC	Ordinary Portland cement
p(d)	Probe perimeter
PDF	Probability density function
PUA	Polyurea waterproof adhesive
PUR	Polyurethane waterproof coating
Ra	Roughness profile
RMS	Root mean square
SEL	Size effect law
SEM	Scanning electron microscope
SF	Silica fume
SiC	Silicon carbide
SNT	Statistical nanoindentation techniques
TEM	Transmission electron microscopy
UHD-CSH	Ultra-high-density gel phase
UHPC	Ultra-high performance concrete
W/C	Water/cement

WOPC	White ordinary Portland cement
XRD	X-ray diffraction

1. Introduction

Cement-based materials (CBMs) are the most widely used building materials and are used to construct infrastructure and buildings because of their good mechanical characteristics and durability. CBMs are heterogeneous on multiple length scales [1], with characteristic length scales ranging from nanoscale to macroscopic scale [2,3]. The multiphase and multiscale features determine the macroscopic (i.e., engineering) properties of CBMs [4], whereas the mechanical properties, volume stability, and durability of concrete are closely related to the nanoscale characteristics of the microstructure [5,6]. For example, C-S-H gel, the main hydration product of cement, exhibits a unique nanoparticle morphology, which can be subdivided into low-density gel phase (LD-CSH), high-density gel phase (HD-CSH), and ultra-high-density gel phase (UHD-CSH) according to its packing density [7]. These forms of C-S-H have different micromorphologies, stacking patterns, and nanomechanical properties, which determines their strength, shrinkage, creep, and service life at the macroscopic level. Understanding the morphology, microstructure, and composition of C-S-H will help clarify the microstructure evolution mechanism of CBMs and design and control their properties. Therefore, it is beneficial to understand the evolution mechanism of the microstructure of hydration products using micro-nanoscale characterization methods, which provides a potential strategy for improving their macroscopic properties.

Modern techniques have provided powerful means for the characterization of the properties of CBMs on smaller scales. Trtik et al. [8] utilized atomic force microscopy (AFM) to determine the local elastic modulus of cement pastes and identified the individual phases present within the cement matrix. Although AFM can be employed to quantify the nanomechanical characteristics of cement pastes, it is difficult to accurately measure unreacted clinker due to the limitations on the testing range of elastic modulus. Wei et al. [9] identified the various phases in cement paste and quantified the porosity of the sample using image processing technology through backscattered electron (BSE) images. However, the information obtained by image processing technology is very limited. For example, it is difficult to quantify the volume fraction of the C-S-H phase with different densities, and challenging to eliminate the influence of subjective factors such as thresholds in the processing process. Vandamme et al. [10] measured the relative volume fractions of C-S-H with different densities in cement pastes with different water/cement (w/c) ratios by nanoindentation and observed that the content of LD C-S-H decreased with increasing the w/c ratio, whereas the content of HD C-S-H and UHD C-S-H increases. There have also been attempts to characterize the interfacial transition zone (ITZ) of CBMs through nanoindentation. Mondal et al. [11] investigated the nanomechanical properties of ITZ between limestone aggregate and matrix by nanoindentation and found that the average modulus of ITZ was approximately 70 % of the matrix. Zadeh et al. [12] studied the ITZ properties between the natural fibers and the cement matrix by nanoindentation and revealed that the ITZ had a porous LD C–S–H gel phase with low hardness and elastic modulus. However, the area probed by a nanoindentation test is too small to obtain representative characteristics, so there is a need to collect a substantial amount of test data for statistical analysis using statistical nanoindentation techniques (SNT), which are both time-consuming and costly. Even with the implementation of newly developed rapid nanoindentation test techniques, it remains essential to statistically analyze a substantial amount of sample data in order to mitigate the slightly unstable results [13]. In addition, the limitations of the indenter size can lead to some specific nanomechanical information that cannot be obtained at a smaller scale by nanoindentation [14,15]. For example, Xu et al. [16] reported that the test results obtained from nanoindentation could not be purely individual phases because of the relatively large volume of the probe used and the interaction involved, whereas finer features such as the size of the interface between unhydrated clinker and C-S-H gel are difficult to precisely detect through nanoindentation. The micro-cantilever testing and micro-column compression methods have been progressively utilized for the characterization of the micro- and nano-scale mechanical properties of CBMs, but their preparation with is very time consuming, and the procedure may influence the properties of the measured phase [17]. Consequently, it is necessary to develop an advanced nanoscale characterization technology that can continuously measure CBMs to obtain more comprehensive and reliable nanomechanical performance information.

The nanoscratch test has been extensively used to characterize the cohesion and adhesion of coatings [18–20], quality of thin films [21–23], strength of ceramics/rocks [24–26], and the damage of metals/polymers [27–29]. The principle of the nanoscratch test is relatively simple: a diamond probe is pressed into the specimen, drawing a trace on the material surface with constant or varying force. Nanoindentation has been widely used in the characterization of CBMs and has also obtained satisfying results, but there are still many shortcomings. Xu et al. [30] found that the width between unhydrated particles and cement paste was too small to be accurately measured by the nanoindentation technique. Fett et al. [31] employed nanoindentation to generate cracks on the surface of the material, subsequently calculating the fracture toughness according to the crack mouth opening displacement. However, due to the relatively small displacements generated by nanoindentation, accurate measurement poses significant challenges. In recent years, an increasing number of studies have employed nanoscratch testing to characterize the nanomechanical characteristics of CBMs [32,33]. Compared to nanoindentation, nanoscratch testing covers a larger testing area on the material surface, allowing for a more continuous and dynamic nanomechanical response over a specified area, which enables abundant data to be obtained [34,35]. Xu et al. [36] studied the effects of nanoSiO_2 on the interface characteristics between unhydrated particles and C-S-H gels in cement pastes by nanoscratch testing. They identified different phases and calculations of the interface widths according to the scratch penetration depth and friction coefficient variations and found that nanoSiO_2 is unlikely to change the interface width, but can enhance the hardness and elastic modulus of the interface. Akono [37] studied the effect of carbon-based nanomaterials on the fracture properties of cement paste by nanoscratch testing. The results indicated that carbon-based nanomaterials can improve the fracture toughness of cement pastes, and the increase in the fracture toughness of the CBMs is positively correlated with the mass fraction of carbon-based

nanofillers. Nanoscratch testing allows for continuous measurement of CBMs to acquire more comprehensive and reliable nanomechanical properties information compared to discrete testing methods, which is characterized by a wide testing range and high testing precision. Wu et al. [38] investigated the friction resistance of concrete surfaces using nanoscratch testing, revealing that the application of polyurethane waterproof adhesive treatments on surfaces can enhance the impact resistance and scratch resistance of concrete. This improvement significantly reduces wear ratios, resulting in lower roughness after abrasion, which contributes to enhancing the erosion resistance of concrete protective structures against debris flows. At present, the nanoscratch technology has been effectively applied to evaluate the fracture properties [39,40], wear resistance [41,42], and interfacial bonding properties [43,44] of CBMs. In addition, the combination of nanoscratch with advanced techniques such as AFM, energy dispersive spectroscopy (EDS), BSE image analysis, and acoustic emission has been applied to characterize the nanomechanical characteristics of CBMs [45]. Therefore, nanoscratch demonstrates considerable potential in characterizing the nanoscopic features of CBMs.

This review aims to comprehensively summarize the applications of nanoscratch technology in characterizing the nanoscale microstructure and nanomechanical characteristic of CBMs. In this review, the fundamental principles of nanoscratch testing are first introduced, followed by a detailed discussion of specimen preparation procedure including specimen preparation steps, requirements, and specific details that require particular attention. Then, a systematic overview of the nanoscratch testing procedure is presented, along with a discussion on determining appropriate nanoscratch parameters including maximum scratch depth, probe type, loading regime, loading mode, etc. The nanomechanical properties derived from nanoscratch tests, including hardness, friction coefficient, elastic recovery ratio and fracture properties, along with the associated experimental results, have been summarized and discussed. Furthermore, recent applications of nanoscratch technology in CBMs are also highlighted, emphasizing its application in phase identification and determining the corresponding volume fraction, exploring tribological features, quantifying interfacial characteristics, and evaluating fracture properties. The combination of nanoscratch and diverse advanced techniques such as AFM, BSE, and acoustic emission is also further discussed to deepen the appreciation of the nanoscale of CBMs. Finally, potential challenges associated with applying nanoscratch technology in CBMs are considered, along with possible solutions. This review provides an effective approach for researchers to better understand the nanoscale characteristics of CBMs, while also supporting the development and promotion of scratch testing techniques.

2. Specimen preparation

The accuracy of nanomechanical characterization can be improved by uniformly flat and smooth specimen surfaces [33]. Due to the shallow penetration depth of the probe in scratch testing (typically 1–2 μm), the test results are strongly influenced by the surface characteristics of the specimen [46,47]. Therefore, the main purpose of specimen preparation is to minimize the roughness of the specimen surface, control specimen perturbation, thereby ensuring reliable and repeatable results in nanoscratch testing [48]. Chen et al. [49] observed that with an increase in surface roughness, the measured nanomechanical properties such as the elastic modulus and hardness of the cement specimens decreased accordingly. Trtik et al. [8,50] reported that higher surface roughness increased the dispersion of the hardness and friction coefficient obtained from testing, which in turn affected the statistical accuracy of the results.

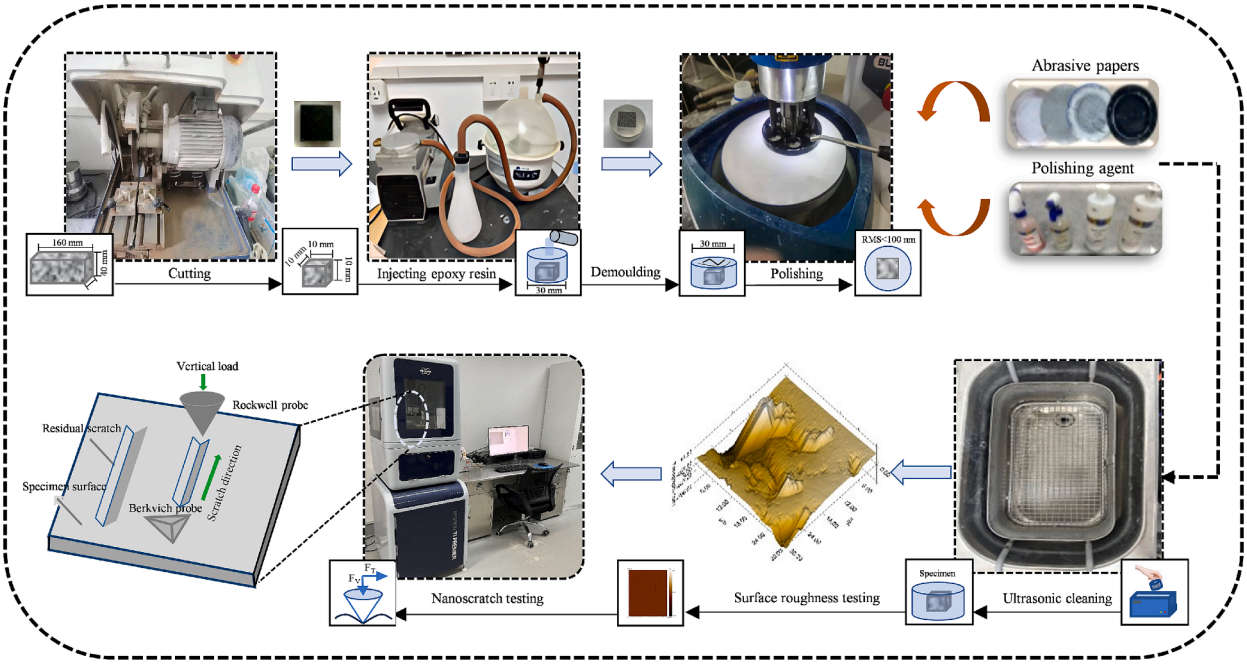

Fig. 1. Scratch specimen preparation and test procedure (Image obtained from author's laboratory).

Xu et al. [30] also found that as the surface roughness of the specimen increases, the feedback error signals during the testing process become more pronounced, leading to greater dispersion in the nanoscratch tests result. Therefore, it is essential to select the appropriate preparation procedure for scratch specimens to minimize the surface roughness.

The specimen preparation process for the nanoscratch test mainly includes specimen cutting, epoxy impregnation, grinding and polishing, ultrasonic cleaning, and vacuum drying, as shown in Fig. 1. According to the standards of ASTM G171 and credible literature [43,51–54], the primary preparation process and schematic representation of cement specimens for nanoscratch testing are summarized as follows (Fig. 2).

The cement specimens are immersed in absolute ethanol or isopropanol to terminate hydration and cut into a suitable size (in general 1–2 cm cubes). Then, epoxy resin is injected into the specimen molds, which remain for 24–48 h before demolding. It is advised to perform the epoxy impregnation under vacuum conditions to prevent residual air pockets in the epoxy resin. However, the vacuum impregnation time should not be too long to prevent epoxy resin from penetrating the microporosity of the specimen and affecting the test results [55]. Khedmati et al. [56] reported that vacuum impregnation of specimens using epoxy resin protected microstructures from cracking during polishing. In addition, epoxy resin strongly adheres to cement specimens, providing structural support during grinding and polishing while also preventing cracking of the sample surface [54]. However, the disadvantage of embedding epoxy resin is that the microstructure of the specimen surface may be changed by the resulting composite medium [51].

After the epoxy has solidified, the specimens are ground with abrasive papers of different gradations (from low to high). Generally, gradations of 200–1200 and 2000–4000 are used for coarse and fine grindings, respectively. For abrasive paper with different gradations, it is recommended that the grinding time be carefully controlled. If the grinding time is too short, the specimen surface can be incompletely exposed. However, too long polishing time may cause specimen damage. To minimize specimen perturbation and create a smooth testing surface, a relatively slow grinding speed is also required [10]. The specimen should then be placed in a cleaning solution that does not react with the cement component and cleaned with ultrasound for 1–5 min [53,57,58].

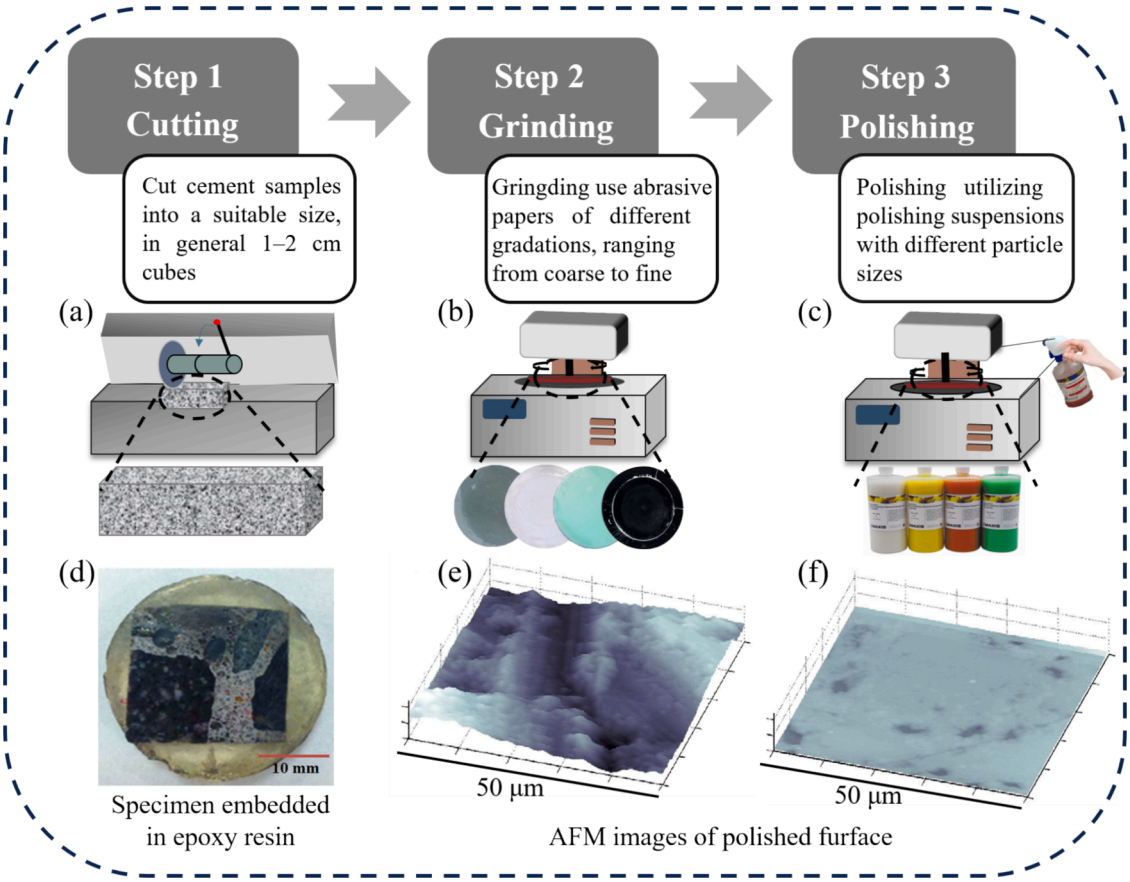

Fig. 2. Three-step representation specimens preparation process for CBM (a) cutting, (b) grinding, and (c) polishing; (d) the specimen embedded in epoxy resin after cutting; the surface microstructural morphology of cement specimen (e) after grinding and (f) polishing (reproduced under license number 5892970322281 and 5892990545545 from Refs. [48,61]).

The ground surfaces remain rough on a microscopic scale, which needs to be polished using polishing suspensions of progressively finer particle sizes to achieve a flat and smooth surface. During the polishing process, when polishing suspensions of different particle sizes are used, the polishing time should be increased sequentially as the polish particles become finer until sufficient smoothness of the specimen surface is achieved. After each polishing step is completed, the specimen needs to be ultrasonically cleaned to eliminate the surface adsorbed polishing particles and the specimen powder produced during grinding [48,59,60]. The specimens should be stored at room temperature under vacuum drying until the scratch test is performed.

Recently, there have been many attempts to improve specimen preparation procedures in nanoscratch testing, summarized in Table 1. Lomboy et al. [62] found that specimens polished with a water-based polishing solution are less damaged and polluted compared with those polished with an oil-based polishing solution. However, water-based polishing solutions may lead to further hydration of unhydrated components. Sakulich et al. [63] reported a method for fine polishing using a range of diamond suspensions of

Table 1
Specimen preparation parameters for nanoscratch testing.

Specimen types	Specimen size (mm)	Curing condition for cement specimen	Grinding and polishing	Ultrasonic cleaning	Roughness (nm)	Ref.
Pure cement paste	Cylinder, 5 × Φ10	Cured for 7 d at 20 ± 2 ℃	SiC abrasive papers (150, 800, and 1500 mesh) grinding, diamond particle suspension (1 um) polishing	Ethanol for 2 min	<400	[57,58]
	Cylinder, 20 × Φ25	Cured for 28 d at 20 ℃			47	[52]
	Cube, 10 × 10 × 10	Cured for 28 d at 20 ℃ and 95 % RH	Abrasive papers (800, 1200, 1500, 2000, 2500, 3000, 4000, and 7000 mesh) grinding for 1 min, diamond particle suspension (3, 1, and 0.25 um) polishing for 30 s	Engine oil	164–294	[54]
	Cylinder, 5 × Φ10	Cured for 28 d	SiC abrasive papers grinding; diamond particle suspension (9, 3, 1, and 0.05 um) polishing for15 min	Ethanol for 5 min		[53,66]
	Cylinder, 8.5 × Φ20	Cured for 7–672 h	Diamond particle suspension (15 and 9 um) grinding and alumina pads (9, 3, and 1 um) polishing	Isopropanol		[60]
	Cylinder, 20 × Φ20	After freeze–thaw, cured in temperature-controlled room for 28 d	SiC abrasive papers (180, 400, and 1200 mesh) grinding, diamond particle suspension (9, 3, 1 and 0.25 um) polishing for 30 min	Ethanol	39	[40]
	Cylinder, 6 × Φ27	Cured in lime water for 4 months at 22 ℃	SiC abrasive papers (2000 and 4000 mesh) grinding, diamond particle suspension (0.25 um) polishing for 30 min	Ethanol for 2 min		[45]
Blend cement paste	Cuboid, 5 × 5 × 3	Cured for 24 h at 20 ± 2 ℃ and 100 % RH	SiC abrasive papers (34.2, 22.1, 14.5, and 6.5 um) grinding for 5 min, diamond particle suspension (6, 3, 1, and 0.3 um) polishing for 30 min	Ethanol for 15 min	23.5	[36]
	Cube, 5 × 5 × 5	Cured in water for 28 d at 20 ± 1 ℃	SiC abrasive papers (500, 800, 1200, 2400, and 4000 mesh) grinding, diamond particle suspension polishing	Ethanol for 5 min	<50	[43]
	Cube, 10 × 10 × 10	Cured in water for 7, 28, 56 d	SiC abrasive papers (52, 35, 22, and 15 um) grinding, diamond particle suspension (9, 6, 3, 1, and 0.05 um) polishing			[68]
	Cylinder	Cured in deionized water for 7d	SiC abrasive papers (240, 400, and 600 mesh) grinding, SiC abrasive papers (1 and 0.25) um polishing	Oil-based solvent		[37]
	Cylinder, 5 × Φ30	Cured in deionized water for 7 d at 20 ± 1 ℃	SiC abrasive papers (400, 600, and 1200 mesh) grinding, diamond particle suspension (3–0.25 um) polishing	Oil-based solvent for 2 min		[70]
	Cylinder, 5 × Φ30	Cured in deionized water for 7 d at 20 ± 1 ℃	SiC abrasive papers (50, 18.3, 10.6, and 7.8 um) grinding, SiC abrasive with particle size (3, 1, and 0.25 um) polishing	N-decane solvent		[71]
Concrete	Cylinder, 5 × Φ32	Cured for 28 d	Abrasive papers (400, 600, 800, and 1200 mesh) grinding for 2 min, diamond particle suspension (3 and 1 um) polishing for 60 and 90 min, respectively	N-decane solvent		[51]
	Cube	Cured for 28 d at room temperature	Abrasive papers (6, 3, and 1 um) grinding for 1 h, diamond particle suspension (0.25 um) polishing for 4 h	Ethanol for 5 min		[72]
	Cylinder		SiC abrasive papers (240, 400, 600, 800, and 1200 mensh) grinding, colloidal suspensions of polycrystalline diamond with particle size (3 and 1 um) polishing	N-Decane solvent		[73]
Geopolymer	Cuboid, 5 × 5 × 3	Cured for 28 d	SiC abrasive papers (360, 600, and 1200 mesh) grinding, alumina pads (1 and 0.3 um) polishing for 20 min			[74,75]

*RH: Relative Humidity, SiC: silicon carbide.

different particle sizes (15, 9, 6, 3, 1, and 0.5 μm) for specimens used for nanoscratch testing. A smooth polished surface was obtained using this polishing method, and the roughness of the specimen surface was successfully controlled below 100 nm. Some studies have proposed that a smaller size range of diamond suspensions were used to polish cement specimens, such as 3–0.25 μm [54,64], 6–0.3 μm [36,65], 6–0.1 μm [65], 9–0.05 μm [63,66,67], and 6–0.05 μm [30,68,69], and lower roughness specimen surfaces were achieved. In addition, Vandamme et al. [10] found that the repeatability of the polishing specimen preparation process can be improved by using only a single particle size (0.5 μm) of diamond suspension.

Finally, the surface roughness of the polished specimens can be examined by AFM to ensure that the roughness complies with the test requirements [48,52,76]. Akono et al. [77] suggested that the surface roughness of the specimen should be controlled to an order of magnitude smaller than the scratch depth (Typically less than 50 μm). However, when evaluating specimen surface roughness with AFM, the average roughness at multiple locations must be calculated to accurately reflect the overall characteristics of the heterogeneous CBMs [50]. In studies by Trtik et al. [50] and Němeček et al. [78], the surface roughness of scratch specimens was calculated using the root mean square (RMS) method (Fig. 3), as shown in Eq. (1).

$$\mathrm{RMS} = \sqrt{\frac{1}{m \cdot n} \sum_{i=1}^{n} \sum_{j=1}^{m} (h_{ij} - h_{mean})} \tag{1}$$

where m and n are the pixel size of the image; h_{ij} is a height reading in pixels (i, j); and h_{mean} is the average of all heights obtained.

The arithmetic mean of the roughness profile (Ra) can be used to calculate the roughness of the specimen surface, as shown in Eq. (2) [48].

$$R_a = \frac{1}{N} \left| Z_j - Z_m \right| \tag{2}$$

where N is the number of data points; Z_j is the height at a particular point (j); and Z_m is the average of the heights of particular specimens.

In addition to the surface roughness of the specimen, scratch test results are affected by different factors during specimen preparation, such as water-based solutions used in cutting, polishing, and cleaning [67]. Kim et al. [80] found that the moisture content in specimens had a remarkable effect on the elastic modulus [80–82], hardness [83,84], and elastic–plastic properties [85] of C-S-H gel. Therefore, prolonged contact with water during specimen preparation should be avoided. For example, Liu et al. [54] used oil instead of water as a polishing solution during the grinding and polishing processes, which prevented further hydration of hardened cement specimens. In addition, if testing is not conducted immediately after polishing, it is recommended that the prepared specimens be stored under vacuum to prevent further hydration or carbonation.

3. Determination of the nanoscratch parameters

Although nanoscratch testing has been mainly applied in single-phase homogeneous materials, a rich theoretical basis for its application in multiphase heterogeneous materials exists [86,87]. Given the microscopic heterogeneous structure of CBMs, the impact of the testing regime must be considered during testing [34]. Therefore, an appropriate probe type, scratch penetration depth, and loading regime need to be considered for nanoscratch testing. In addition, to avoid interference between different scratches, a reasonable scratch spacing should be selected. The material information, including specimen types, materials composition, water/binder ratio, and the test parameters, including probe types and loading regime, are summarized in Table 2.

3.1. Maximum scratch depth

At the initial stage of load, the load is minimal (typically, <20 μN), resulting in a shallow scratch. However, when the vertical load

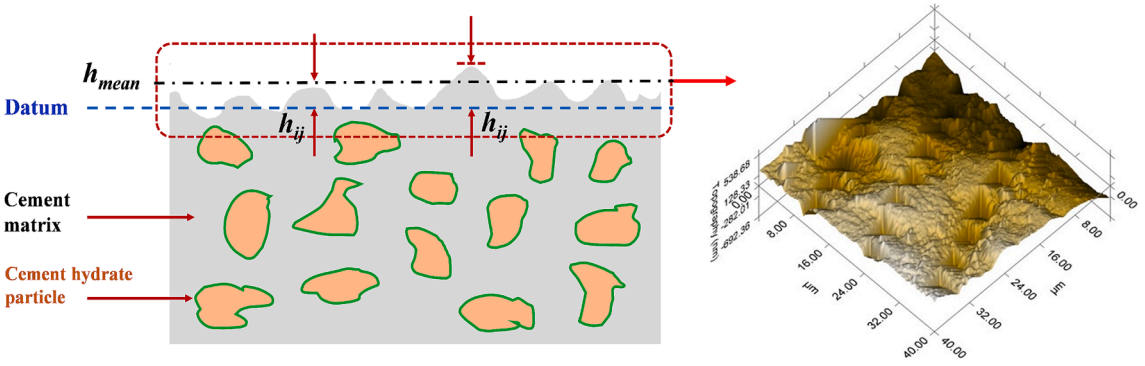

Fig. 3. Surface roughness quantified using the RMS method (reproduced under license number 5893010034811 from Ref. [79]).

Table 2
Materials information and test parameters for the nanoscratch testing of CBMs.

Specimen types	Materials composition	Water/solid ratio	Loading mood	Loading speed (μm/s)	Scratch length (μm)	Number of scratches	Scratch spacing (μm)	Probe type	Reference
Pure cement paste	Clinker	0.25 0.30	4 mN (CL)	10	200			Berkvoich	[58]
	Clinker	0.30 0.40	8 mN (CL)	10	200	3		Berkvoich	[57,88]
	OPC	0.30	14 mN (LIL)	8	100			Berkvoich	[52]
	OPC	0.30	10 mN (LIL)		100	6		Berkvoich	[40]
	OPC	0.40	200 mN (CL and LIL)					Berkvoich	[54]
	White OPC	0.40	30 N (LIL)	100	3	7 – 17		Rockwell	[60]
	OPC	0.40	100 mN (LIL)	15				Rockwell	[89]
Blend cement paste	OPC with 1 wt% nanoSiO_2	0.28	8 mN (CL)	0.5	12	>10		Berkvoich	[36]
	OPC with 35 wt% silica fume	0.45 0.58	(DCL)			16		Flat punch blade	[32]
	OPC with 35 wt% silica fume	0.45	30 N (LIL)		3	>6		Rockwell	[90]
	OPC with 2 wt% nanoSiO_2 or OPC with 0.08 wt% carbon nanotubes	0.30	10 mN (CL)	1	<100	6		Berkvoich	[76]
	OPC with silica fume and carbon fiber	0.19	1 mN	0.4	10	10		Rockwell	[43]
	OPC with 0.3 wt% short multi-walled carbon nanotubes	0.35	15.5 mN (LIL)		100			Berkvoich	[91]
	OPC with 0.1 %wt, 0.2 % wt and 0.4 %wt carbon nanotubes	0.40	50 mN (CL)	2	100			Berkvoich	[54]
	High alumina cement, poly, glycerol, and deionized water	0.11	30 N (LIL)	100	300	8		Rockwell	[67]
	OPC with 0.1–0.5 wt% carbon-based nanofillers	0.44	2.5 N (LIL)	100	5000	7	1200	Rockwell	[37]
	OPC with 0.2 wt%, 0.5 wt % and 1 wt% multi-walled carbon nanotubes	0.44	4 N (LIL)		5000	8		Rockwell	[70]
	OPC with 1 wt% and 5 wt% Nano-TiO_2 particle	0.44	2 N (LIL)			12		Rockwell	[71]
	OPC with 1.0 wt% C-A-S-H nano-seeds	0.40	100 mN and 200 mN (LIL)	15		9		Rockwell	[89]
Concrete	OPC with river sand as FNA	0.50	1 mN (CL)	25	200		25	Berkvoich	[72]
	The gel produced by the alkali-silica reaction		10 N(LIL)		2000		2000	Rockwell	[51]
	OPC with crushed dolomitic limestone as CA and natural river sand as FNA	0.20 0.30	2 mN (LIL)	0.5		10	50	Berkvoich	[53]
	OPC with FNA and CA and rubber powder	0.44	15 N (LIL)	100	3			Rockwell	[73]
	OPC and FA as binder, crushed limestone as CA and natural river sand as FNA	0.40	8 mN (CL)		200	6	60	Berkvoich	[41]
Geopolymer	Low calcium FA with alkali solution and limestone as aggregates	0.57 0.33	4 mN (CL)	4	100		4	Rockwell	[74,75]

*CA: coarse aggregate, FNA: fine aggregate, OPC: Ordinary Portland cemen; LIL: linearly increasing loading, CL: constant loading, DCL: displacement-controlled loading, FA: fly ash.

increases, the scratch depth gradually increases and tends to be stable. For example, it has been reported that a 600 nm Berkovich indenter used in nanoscratch testing achieves an average penetration depth of 466 nm in C-S-H gel when subjected to a vertical load of 4 mN [92]. In certain specific scenarios, when the maximum load reaches 50 mN, the corresponding scratch depth can even exceed 1 μm [68]. Under identical load conditions, the instantaneous scratch depth is related to the hardness of the tested materials. Specifically, a greater scratch depth indicates a decrease in material hardness. Liu et al. [54] found that scratch depth is highly sensitive to the

hardness of local phases, which suggests that scratch testing may be a preferred method for characterizing CBMs with varying hardness phases. To ensure that the scratch test results are not dependent on any specific characteristic length and the precise nanomechanical properties of individual phases can be effectively distinguished, the maximum scratch depth (h_{max}) should comply with Eq. (3) [7].

$$d < h_{max} < \frac{D}{10} \tag{3}$$

where, d is the maximum heterogeneous size of the material, which is approximately 1–5 nm. For C-S-H gel, the characteristic value of d refers to the size of the individual gel particles or the size of the pores within the gel at a similar scale, which is determined to be 5 nm. If $h_{max} < d$, the scratch depth is too small, and the test results are influenced by the heterogeneous characteristics of the phase itself. D is the characteristic size of the microstructure. If $h_{max} > D/10$, the scratch depth is too large, and the test results are influenced by the interaction of individual phases inside the material. However, the value of D is still controversial, as the microstructure of CBMs is influenced by factors such as mixture proportions and the hydration degree. For hydrated cement specimen with a w/c ratio of 0.5, Richardson et al. [93] found that D was about 1–3 μm by transmission electron microscopy (TEM), but the value of D observed by Ulm et al. [94] was about 10 μm using BSE image analysis. Therefore, the h_{max} of CBMs should be controlled in the range of 100–20000 nm.

3.2. Types of scratch probes

Depending on the test purpose and tested material characteristics, different types of probes can be used. Commonly used nanoscratch probes include rectangular blade probes, conical probes, spherical probes, three-sided pyramidal probes, four-sided pyramidal probes and sphere-conical probes. The schematic representation of probes used to perform scratch testing are presented in Fig. 4. Rectangular blade probes [27,82] are typically used to characterize the fracture properties of materials (e.g. shale, mudstone, metals, etc.) at relatively high loads (e.g. 30 N) [33,95]. The three-sided pyramid probes and the sphere-conicals are extensively utilized in nanoscratch testing of CBMs. The Rockwell probe is the most widely used spherical conical probe with a symmetrical geometric shape and a robust diamond probe tip, resulting in less tested material wear [77,96]. The Berkovich probe is the most widely used three-sided pyramidal probe, which has the advantage of allowing better control of the scratch depth and more accurate access to the nanomechanical properties of individual phases [36,62]. However, due to the three-sided pyramid shape of the Berkovich probe, anisotropic stress distribution and deformation of the material can be generated during scratch testing [97]. Compared to Berkvoich probes, the Rockwell probe has more higher degrees of freedom in geometry, which avoids errors due to different probe orientations in repetitive testing [75,95]. Some studies have reported the effect of different Berkvoich probe orientations scratching on coefficient of friction (COF) values and found that the different test orientations of the probe resulted in COF values ranging from −0.37 to 0.57 [98,99].

3.3. Loading regime

The nanomechanical properties of CBMs are closely related to the loading regime during the process of nanoscratch testing, including parameters such as loading levels and loading rates, and scratch length. The loading regime typically consists of three steps, as presented in Fig. 5(a). The first step is pre-scanning, where the test area is scanned and preliminary surface information about the

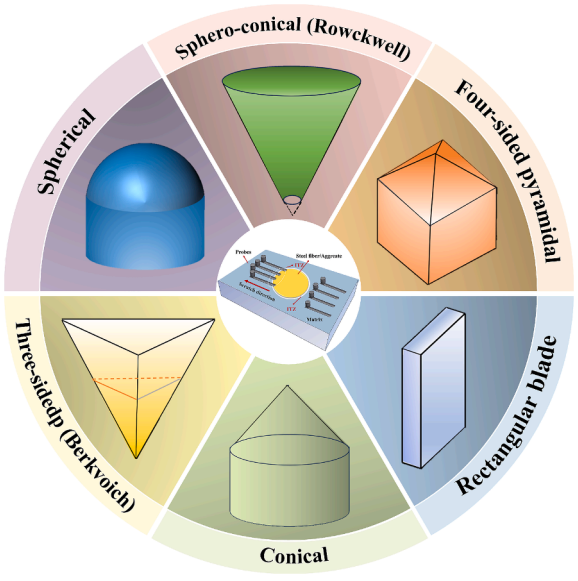

Fig. 4. Schematic representation of probes used to perform scratch testing.

specimen is provided, including the location of scratches, and surface characteristics. Generally, the loads used for scanning are small enough (typically, <20 μN) not to cause damage or permanent deformation of the specimen [53]. Then, the nanoscratch test is performed by imposing a target load on the testing area while scratching with a specified speed. During the scratch process, the probe tip follows the same paths three times, simultaneously monitoring and recording both normal displacement and normal force [53,92]. Finally, there is a post-scanning, where the residual scratches are scanned again with a very light load (typically, <5 μN), and the depth of the residual scratches is measured. Liu et al. [54] investigated the influence of the loading regime on the nanomechanical properties of CBMs, which include both various loading rates (5, 10, and 20 mN/s) and loading levels (ranging from 10 to 200 mN). They discovered that for the same material, a higher scratch loading rate and loading results in a smaller penetration depth of the scratch, which contributes to an increased measured hardness. In addition, Wei et al. [52] reported that a lower vertical loading rate can reduce the fracture toughness of the clinker phase in CBMs. Němeček et al. [45] also reported similar research results, indicating that with increasing load levels (from 200 to 500 mN), the measured fracture toughness of the cement paste correspondingly decreases.

A perfectly smooth surface with negligible roughness is impossible to be achieved, because of the heterogeneous feature of CBMs. Based on the pre-scan profile, the surface roughness and inclination of the specimen can be determined (Fig. 5(b)). Therefore, it is necessary to pre-scan the cement specimen surface before scratch testing. Then, the pre-scan data is subtracted from the scratch data to acquire the information necessary for scratching on a flat surface [88,101]. In addition, after the scratch testing, due to the elastic recovery of CBMs, post-scanning is also required to acquire the depth of residual scratches and the elastic recovery. The plastic deformation of the CBMs can be determined by measuring the residual scratch depth, while the elastic recovery properties can be assessed through the difference between penetration depth and residual scratch depth.

3.4. Loading modes

The nanoscratch system is equipped with two sensors, one measures the force (vertical force) and displacement in the direction of penetration, while the other records the force (transverse force) and displacement in the direction of movement [92]. For nanoscratch testing, displacement-controlled loading (DCL) and force-controlled loading (FCL) are the most typical loading modes. The DCL mode controls the normal displacements of the probe during scratch testing while recording transverse and vertical loads. Specifically, in the DCL mode, the scratch testing system automatically and accurately adjusts the position of the scratch probe based on preset displacement parameters, which include both scratch length and depth profiles. The DCL mode ensures precise control of vertical displacement during scratching process, which has been extensively utilized to determine the wear and scratch resistance of CBMs [102]. The FCL mode controls the vertical loads while recording normal displacements and transverse loads. Specifically, in the FCL mode, the scratch testing system automatically adjusts the vertical load applied by the scratch probe based on preset force parameters. The FCL mode ensures precise control of the load during the scratching process, enabling it to capture subtle responses of materials under minor loads, which contribute to revealing the mechanical behavior of CBMs at the nanoscale [74,76]. Changes in stress, strain, and hardness of materials during friction in scratch tests can be evaluated by load–displacement curves obtained in both loading modes. In addition, depending on the form of loading application, the linear incremental loading (LIL) routine [37,51–53,60,67,73,90,91] and constant loading (CL) routine [57,58,72,74–76,88] are the main routines for FCL loading modes.

Fig. 6 (a and b) presents the representative scanning electron microscope (SEM) images of scratched grooves in cement paste with the CL and LIL routines. The depth and width of the grooves gradually increased during LIL scratches, while the depth and width of the straight grooves remained similar during CL scratches. Liu et al. [54] compared the hardness distribution of the CL and LIL loading routines at the identical loading level. Compared with the CL loading routine, the LIL loading routine produced more peaks in the interface (Fig. 6(c)). This is because, in the CL routine, a constant vertical force is imposed on the overall length of the scratch, so that

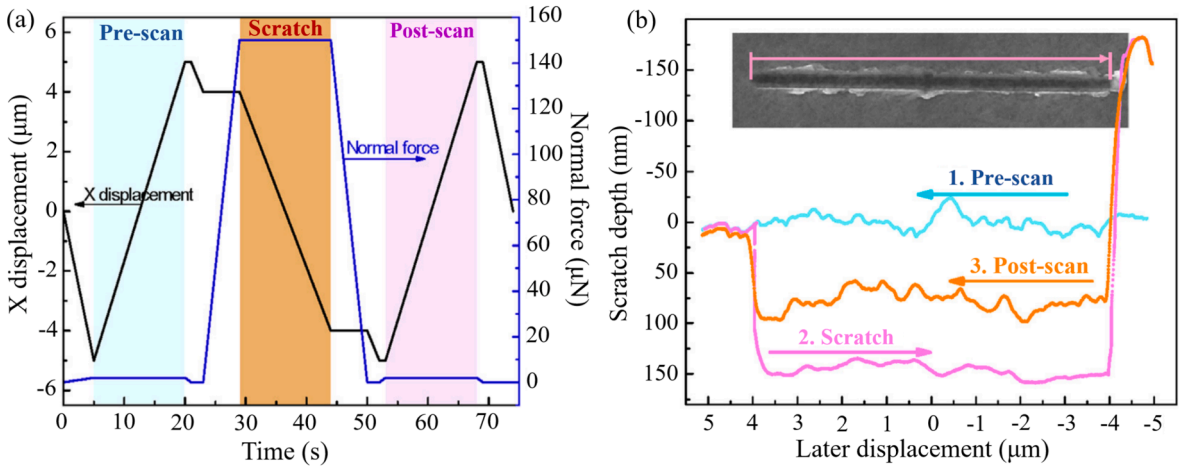

Fig. 5. Testing procedure of nanoscratch [100] (a) loading regime and (b) the scratch depth distributions of pre-scan, scratching, and post-scan along the scratch path (reproduced under license number 5893010771141 from Ref. [100]).

the assessed hardness spectrum accurately reflects phases along the scratches. However, in the LIL scratches where the imposed forces increased to a constant value, scale crossover always occurs, and LIL scratch hardness spectra exhibit significant peaks in the interface. The study found that the LIL routine is capable of detecting more phases or obtaining more detailed information regarding the nanoscale features of CBMs, compared to the CL routine.

3.5. Other parameters

Considering the heterogeneity of the microstructure of CBMs, a sufficient amount of data is required to be collected for statistical analysis in scratch testing, while the randomness of the selection of the test area is also crucial to ensure the reliability of the results. Liu et al. [54] proposed the use of 100 data points for statistical analysis, with an error margin that can be maintained within ± 5 %, which is considered an acceptable outcome. It is also recommended that three or more areas be selected for the scratch test [57]. Kimm et al. [103] reported that the standard deviation of scratch hardness showed a decreasing trend with increasing scratch length. Therefore, it is recommended to use relatively long scratch lengths [53]. A sufficient amount of data and the length of the scratch test can result in the data being statistically representative. In previous studies, the scratch length was typically chosen to be 10 μm or larger, in some cases reaching up to 200 μm [58,73,88]. Reasonable scratch spacing can prevent the interaction between scratch points in the nanoscratch test. For example, Zhao et al. [53] conducted a total of 10 scratch tests on each cement specimen, with a scratch length of

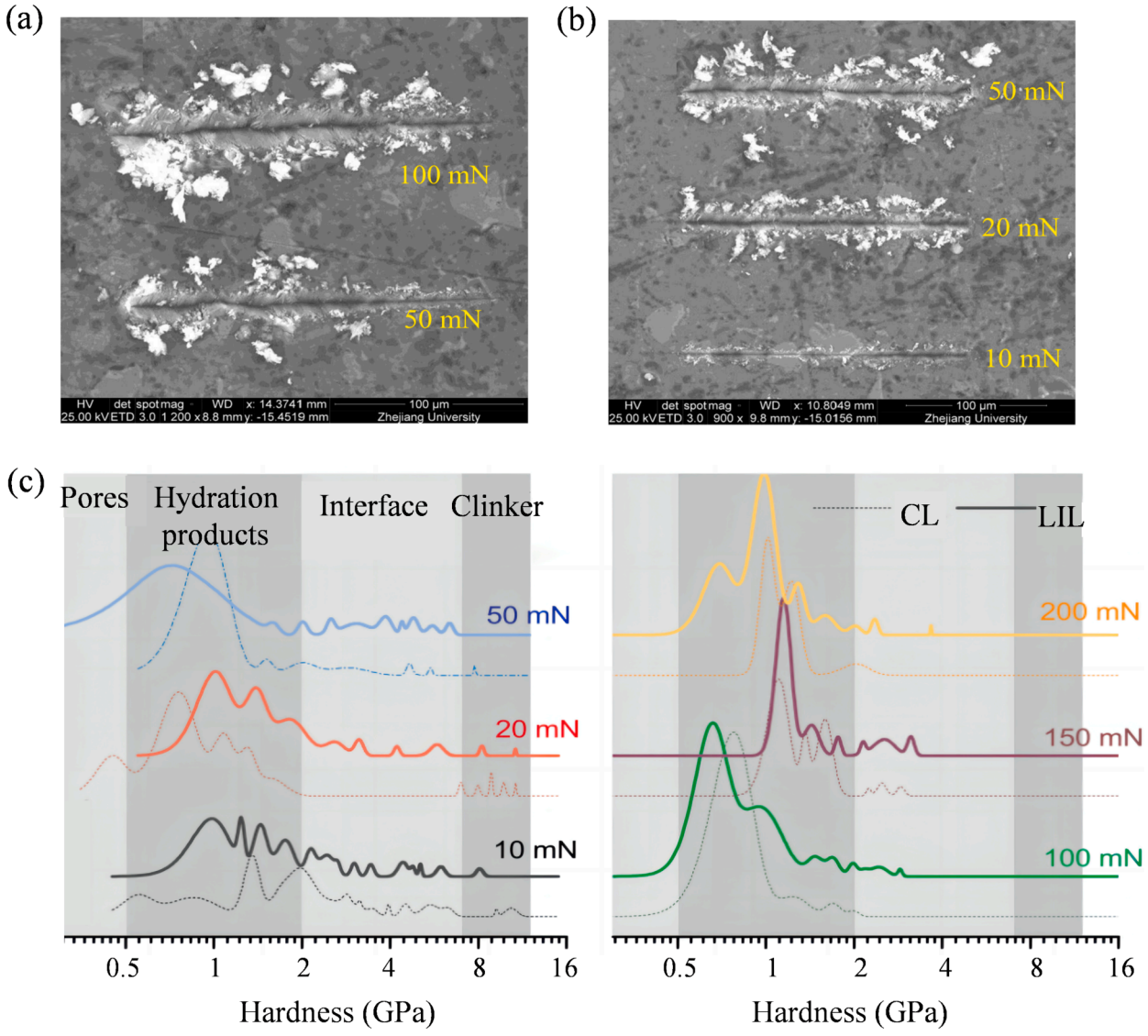

Fig. 6. Microscopic morphology of the LIL (a) and CL (b) scratched grooves; hardness distributions of CL and LIL routine at different loads of 10, 20, 50, 100, 150, and 200 mN (c) (reproduced under license number 5893011420190 from Ref. [54]).

10 μm and a spacing of 50 μm between adjacent scratches, resulting in relatively stable and reliable scratch data. In addition, scratch tests should be conducted in a stable and sound proof environment considering the effects of environmental factors such as vibration, temperature, and humidity changes. The effect of thermal drift on scratch test data should also be considered and corrected accordingly.

4. Nanomechanical properties obtained from nanoscratch testing

4.1. Scratch hardness

Scratch hardness is a frequently employed parameter for evaluating the scratch performance of materials, which can be reflected through the penetration depth of the tested material. The lower the hardness, the greater the penetration depth [104]. At present, there are two definitions of scratch hardness, which are calculated as shown in Eqs. (4) and (5) [54].

$$H_S = \frac{F_V}{A_P} \tag{4}$$

$$H_P = \frac{F_T}{A_{LB}} \tag{5}$$

where H_S is the ordinary scratch hardness; H_P is the ploughing hardness; F_V is vertical load; F_T is transverse load; A_P is the vertical area projection; and A_{LB} is the contact area.

Even for the same material, the scratch hardness and indentation hardness may be different [105]. Williams et al. [106] found that the ratio of indentation hardness to scratch hardness increased from 0.6 to 1.4 when the angle of the probe was increased from 90° to 180°. Liu et al. [54] investigated the correlation between ordinary scratch hardness (H_S) and ploughing hardness (H_P) under different load levels and found that the ratio of H_S to H_P was stabilized with a distribution between 0.6 and 2.0 when a load larger than 10 mN was applied to the cement paste. Insufficient load levels can result in instability in the measured H_S and H_P values. In addition, the distribution characteristics of the constituent phases of CBM can be obtained by analyzing the hardness information acquired from the scratch test, utilizing frequency statistics and probability distributions [58,88,107]. However, in order to enhance the precision of the test results, the surface roughness needs to be strictly controlled. Xu et al. [57] studied the hardness and the elastic modulus of cement paste through the penetration depth during scratch tests, and the results were statistically analyzed. According to the deconvolution results, the components (clinker, hydration products, and porosity) in the cement paste were identified and their volume fractions were calculated, and it was found that the volume fraction obtained by the test was consistent with the theoretical results.

4.2. Coefficient of friction

In scratch testing, the COF is often used to evaluate the frictional characteristic of materials [108], which can be defined as the ratio of lateral force (F_T) to the normal force (F_V), as shown in Eq. (6).

$$\mathrm{COF} = \frac{F_T}{F_V} \tag{6}$$

Typically, COF can be considered as the combination of ploughing friction and adhesive friction between the probe and the material surface. For the same specimen or specimen with a completely smooth surface, the coefficient of adhesive friction remains consistent [109,110]. Therefore, the ploughing friction is the primary factor determining the COF value. Specifically, the COF can increase with the ploughing depth of the probe [88]. Akono et al. [73] reported that, when the scratch load increased tenfold, the measured COF of hardened concrete increased by approximately 16 %. This increase is primarily attributed to the greater plowing friction resulting from the elevated vertical load. It is noteworthy that the COF of CBMs remains unaffected by changes in scratch speed.

Understanding changes in COF during scratch testing is a particularly challenging task when analyzing scratch test results. COF is affected by several parameters, including the failure mode of the material, plastic deformation, surface roughness, and test conditions [98,99]. Lee et al. [111] reported that the deformation and failure modes of materials during scratching were analyzed through the method of extracting COF constituents. During the scratch testing process, the non-linear increase of normal and lateral forces causes a variation of the COF with penetration depth. Xu and Yao [88] investigated the tribological properties of cement composites (cement paste and geopolymer) at the nanoscale using nanoscratch testing. The findings indicate that, aside from factors such as surface roughness of the samples and inherent instrument errors, there exists a negative correlation between the COF and the penetration depth of the probe, which has also been further confirmed in other research [73,112]. This is because, as the penetration depth increases, the evolution of the stacking in the direction of the probe scratching contributes to the increasing of the lateral force. Furthermore, due to the strong positive correlation between the wear resistance of materials and COF, COF is extensively employed as a standard for assessing the wear resistance of tested materials [53,113]. Du et al. [41] reported that the incorporation of an appropriate amount of graphene oxide (GO) can significantly enhance the COF of high-volume fly ash concrete, thereby improving its macroscopic wear resistance. However, it is crucial to emphasize that the utilization of COF to characterize material properties should be cautious, as the accuracy of COF measurements is greatly affected by the parameters of the scratch test and the characteristics of the tested materials.

4.3. Elastic recovery ratio

In scratch testing, the probe is pressed into the material under load and the difference between the scratch test and pre-scanning displacements is defined as the total deformation of the material. The elastic deformation is defined as the difference between the penetration depth (h_i) and the residual scratch depth (h_r) during the scratch test. Both the penetration depth and the residual scratch depth are the mechanical response parameters of the material during scratching [53,57], whose tribological characteristics can be revealed through the penetration depth and elastic properties can be speculated from the residual scratch depth. Bucaille et al. [114] first proposed the concept of elastic recovery ratio (ERR), which was defined as the ratio of elastic deformation to total deformation (Eq. (7)).

$$\mathrm{ERR} = \frac{h_i - h_r}{h_i} \tag{7}$$

The deformation of the material can be categorized into elastic deformation and plastic deformation During the nanoscratch testing. Liu et al. [54] discovered that at low scratch loads (e.g. 50 mN), the CBMs primarily undergo elastic deformation. This means that most of the deformation can recover after scratching, resulting in a relatively high ERR. Anderson and Akono [67] conducted nanoscratch tests coupled with SEM image analysis and observed that, when the penetration depth increased, the material surface gradually exhibited plastic deformation, ultimately resulting in fracture. This phenomenon reveals that CBMs are undergoing a transition from elastic to plastic deformation during the process of increasing scratch penetration depth. Therefore, the ERR of the scratched materials is determined by the material characteristics and the maximum scratch depth. In addition to characterizing the elastic characteristic of materials, ERR can also be used to identify the phase distribution in CBMs. Xu and Yao [88] studied the elastic–plastic deformation of cement paste on the nanoscale. The results indicated that the ERR of the unreacted phases and hydration phases in cement pastes with a w/c ratio of 0.3 were about 60 % and 30 %, respectively. In addition, the ratio of hardness to elastic modulus (H/E) is also closely related to ERR [115]. A relatively high H/E ratio (>0.1) indicates that the material has a high elastic deformation during scratch testing [19]. Therefore, the combination of ERR values and H/E values can be employed for evaluating the nanomechanical properties of CBMs.

4.4. Fracture properties

In addition to obtaining the nanomechanical characteristics of materials, the nanoscratch technique also provides a novel approach for measuring the fracture properties of materials. Fracture toughness (K_C) is the capacity of a material to resist crack extension when subjected to external stress impacts. Based on the theory of linear elastic fracture mechanics (LEFM), the Airy stress function is employed to obtain the stress and displacement fields, and the energy release rate is obtained by the J-integration method [60,107,116], as shown in Eqs. (8) and (9).

$$\int_{(s)} \sigma \mathrm{ndS} = \mathrm{F_T e_x} - \mathrm{F_v e_z} \tag{8}$$

$$G = \frac{1 - \mathrm{v}^2}{\mathrm{E}} \frac{\mathrm{F_{eq}^2}}{2pA} \tag{9}$$

where, $E^*=E/(1-\nu^2)$ is the elastic modulus of plane strain; E is Young's modulus; and ν is Poisson's ratio. F_{eq} is the equivalent force, including the normal force (F_v) and the lateral force (F_T).

The application of the principles of LEFM and the J-integral to scratch testing analysis has enabled the correlation of the force and groove geometry with the plain strain fracture toughness, as shown in Eq. (10) [60,90,117].

$$\mathrm{K_c} = \frac{\mathrm{F_{eq}}}{\sqrt{2p(d)A(d)}} \tag{10}$$

where *p(d)* is the probes perimeter and *A(d)* is the projected contact area of the probe orthogonal to the scratching direction. When the probe is inclined, i.e., the angle between the scratch direction of the probe and material surface (θ) > 0, the contributions of F_v to material fracture is evident, as shown in Eq. (11) [96].

$$F_{eq} = \begin{cases} F_T & If\theta = 0 \\ \sqrt{F_T^2 + \frac{1}{2}\frac{(4\in^2 + \in +1)(2\in +1)(3\in +1)}{\in(\in +1)(4\in +1)(5\in +1)} F_V^2} & If\theta > 0 \end{cases} \tag{11}$$

Where $\in$ is a single variable determined by the shape of the scratch probe. For conical probe, $\in$=1; For spherical probe, $\in$=2; and for flat punch, $\in \to \infty$.

For the sphero-conical probe, *p(d)* and *A(d)* are greatly affected by scratch test depth, and further parameter calibration may be required before scratch testing (See Eq. (12)) [60,96].

$$\frac{2p(d)A(d)}{R^3} = \frac{F_T^2}{R^3K_C^2} = \alpha\left(\frac{d}{R}\right)^3 + \delta\left(\frac{d}{R}\right)^2 + \gamma\left(\frac{d}{R}\right) \tag{12}$$

Where, α and δ is the conical and spherical scaling, respectively; γ is the bluntness factor of the probe; and R is the tip radius of the sphero-conical probe.

A quantitative characterization model for fracture toughness was proposed by Akono et al. [107,118] using the LEFM framework. However, Lin and Zhou [119] reported that LEFM can only be applied asymptotically when the probe penetration depth is large enough. Greater penetration depths were often difficult to achieve during scratch testing. To solve this problem, Akono and Ulm [120] applied optical microscopy and SEM to further investigate the fracture failure behavior of CBMs under scratch testing. The robustness of the LEFM scratch model was tested by finite element simulations, and a multi-scale method suitable for the fracture process of CBMs was proposed. The fracture toughness of CBMs is determined by plotting the quantity $F_T/(2pA)^{1/2}$ under the LIL scratch mode. These plots are converged on a horizontal curve, which could be identical to the fracture toughness of CBMs [60,77] (Fig. 7(a)). In the initial phase of the scratch testing, there is some deviation due to the small penetration depth, which may be caused by local plastic deformation of the CBMs rather than fracture failure. Yao et al. [89] also discovered that the interval of fracture toughness of cement paste on the $F_T/(2PA)^{1/2}$ curve coincided with the scratch lengths of fracture failure under SEM images (Fig. 7(b)). The results further confirmed that the $F_T/(2pA)^{1/2}$ value of the cement pastes after fracture failure is the fracture toughness value.

The energetic size effect law (SEL) has been applied to characterize the stress redistribution and release of stored energy caused by fracture process in CBMs [95]. Several studies have suggested that the SEL could be used to determine the relationship between the strength and fracture properties in scratch tests [95,119,121].

$$\sigma_N = \frac{Bf_t'}{\sqrt{1+\frac{\Lambda}{\Lambda_0}}} \tag{13}$$

where, σ_N is nominal strength; B is a dimensionless parameter; Λ is the nominal size of the structure; Λ_0 is transitional length; and f_t' is the tensile strength of the material.

The SEL model serves as a suitable criterion to differentiate between the strength-dominated and fracture-driven scratching processes. Akono et al. [95,122] found that SEL methods can precisely capture the decrease in nominal strength as the ratio of the nominal size of the structure to transition length (relative structural size) increases (Fig. 8). He and Xu [123] employed SEL to identify the critical ductile-to-brittle transition depth for inhomogeneous materials. They found that the strength of the rock at ductile failure and the fracture toughness at brittle failure can be quantified. Similar results were obtained by Hubler and Ulm [121] in CBMs.

5. Application of nanoscratch in cement-based materials

5.1. Phase identification

Cement paste is a multiphase composite which includes various gel phases, calcium hydroxide (CH), unhydrated cement clinker (C_3S, C_2S, C_3A, and C_4AF), and pores. The gel phases are further divided into LD-CSH, HD-CSH, and UHD-CSH, which have different micromorphologies, packing patterns, and nanomechanical characteristics at the nanoscale. For cement paste containing phases with various nanomechanical properties (e.g., elastic modulus, hardness, and fracture toughness), the material micro/nanostructure can be

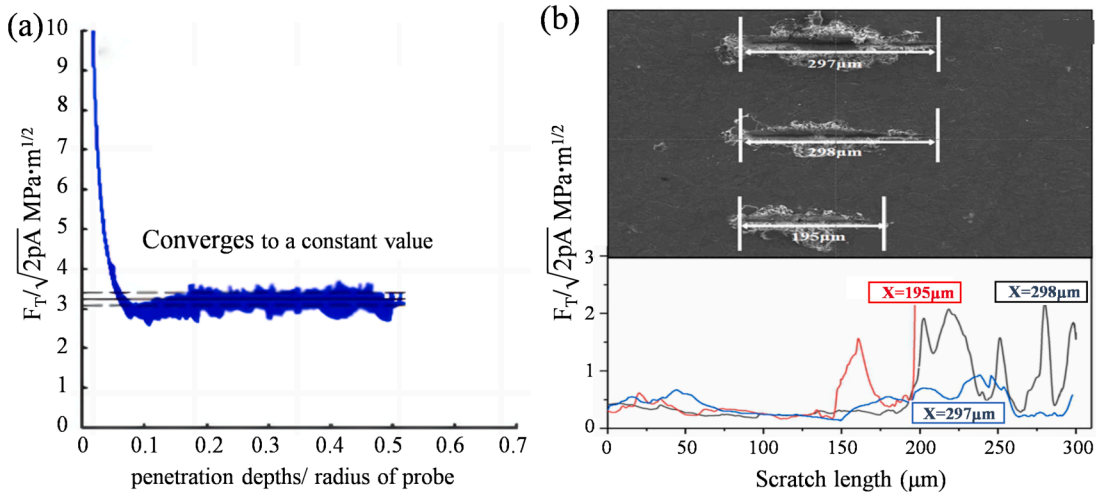

Fig. 7. (a) Convergence to a constant for a cement pastes with a w/c ratio of 0.4 (b) SEM image of cement pastes scratches and corresponding fracture toughness-displacement curves (reproduced under license number 5893020605013 and 5893021118938 from Refs. [60,89]).

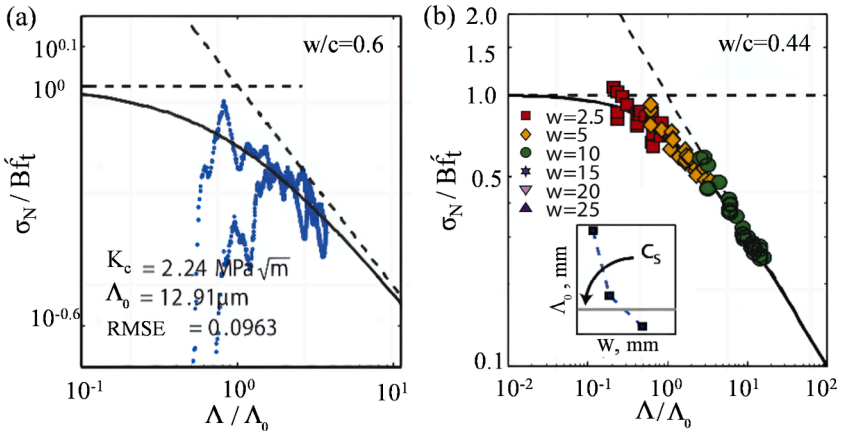

Fig. 8. SEL plots of scratch data of cement pastes with different penetration depth, (a) w/c = 0.60 (b) w/c = 0.44 (reproduced under Creative Commons license from from Ref. [95], and reproduced under license number 5893040526139 from Ref. [122]).

determined from some parameters on the scratches responses of those phases (e.g., scratch penetration depth, lateral force, and residual scratch depth). Therefore, nanoscratch testing can be applied for phase identification, obtaining the volume fraction of individual phases, and investigating the microstructure and nanomechanical characteristics of CBMs.

Xu and Yao [57,88] quantitatively investigated the tribological characteristics of cement paste at nanoscale by nanoscratch testing. Three nanomechanical parameters (depth of penetration, COF, and ERR) closely correlated with the hardness and elastic modulus are obtained during nanoscratch testing, which were analyzed statistically using the deconvolution method through a Gaussian probability distribution (Fig. 9(a)). The results indicated that the phases in the cement pastes (clinker, hydrated products, and pores) had been successfully identified, and their volume contents were found to be consistent with the theoretical predictions of the cement hydration reaction (Fig. 9(b)). However, the mixture of C-S-H and CH can only be distinguished as a mixed phase and not as individual phases because there is little difference in elastic modulus or hardness values between them. In addition, to avoid the effects of different test parameters and the surface roughness of the specimen, Wei et al. [52] proposed the concept of vertical loading rate for phase identification. This was achieved using the slope variation of the curves of either lateral force (F_T) vs. scratch length (L) or variation of penetration depth (d^2) vs. scratch length (L) along the scratch path. The clinker, hydration products, and interface in the cement paste were successfully identified according to the slope of the corresponding stages in the curves. The d^2-L curve has a large slope difference among phases, which is considered to be a reliable parameter for phase identification.

However, nanoscratches still face some challenges in the quantitative characterization of the content of individual phases. Liu et al. [54] obtained the volume fractions of hydration products, unhydrated particles, and pores in cement pastes by nanoscratch testing, Powers model predictions, and BSE image analysis, respectively. It was discovered that the volume fraction of the unhydrated phase obtained by scratch testing was significantly lower than that estimated by BSE analysis and Powers model predictions. This is because scratch testing is still a one-dimensional approach, capable of obtaining load–displacement data only along pre-defined lines, which may lead to deviations in the test results. Therefore, this issue can be addressed by increasing the number of nanoscratches in various orientations or by extending the scratch length to cover a larger area.

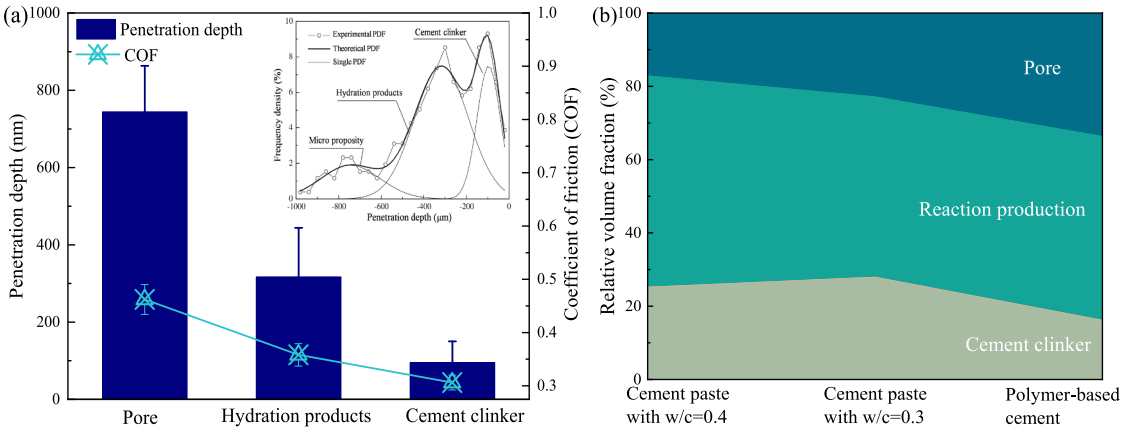

Fig. 9. Results of scratch tests (a) average penetration depth and COF of various phases in cement pastes with w/c = 0.4 and (b) volume fraction of individual phase (data reused under license number 5894120170316 from Ref. [57]).

Krakowiak et al. [14] thought that since nanoindentation and nanoscratch tests are only inferred based on mechanical responses, which may not be suitable for characterizing material phases with different compositions but similar mechanical responses. For example, concrete exposed to the marine environment is easily eroded by seawater, leading to the aragonite and brucite being produced. In scratch tests, aragonite and brucite exhibit similar scratch profiles, and have similar hardness, making it difficult to differentiate between them by scratch testing alone [124]. Therefore, combining scratch testing with other advanced techniques (e.g., BSE image analysis, nanoindentation, and EDS elemental analysis) has been used to help identify phases that have similar mechanical responses to acquire nanomechanical properties results of targeted phases. Palin et al. [72] combined scratch testing with BSE technology to study marine exposed concrete, which found that aragonite and brucite clearly exhibit different grey scale values in BSE images, but similar scratch profiles were exhibited in scratch testing for them (Fig. 10). Combining scratch testing and BSE, the mortar matrix, aragonite, and brucite mineral layers in marine exposed concrete can be distinguished. Although a strong correlation existed between the nanoscratch and image analysis, differences do remain. The mechanical information obtained from nanoscratch cannot be directly compared with the chemical information offered by BSE image analysis [125]. In addition, the quantitative relationship between nanoscratch and test results from chemical analysis techniques is still unclear and needs to be further explored.

5.2. Tribological properties

Abrasion tests are repeatable nanoscratch tests conducted on a single scratch path, where the abrasion depth parameter is mainly applied to characterize the abrasion resistance of specimens [41]. Zhao et al. [53] conducted abrasion testing on high-performance concrete (HPC) and ultra-high performance concrete (UHPC) by nanoscratch testing to evaluate the abrasion resistance, where a greater depth of wear implies a lower abrasion resistance. The results showed that the final wear depth of HPC was 3.14 mm, while UHPC was only 2.04 mm, and the abrasion resistance of UHPC was found to be 54 % higher than that of HPC (Fig. 11(a and b)). Because the abrasion resistance of CBMs is closely correlated to their hardness/stiffness, phases processing higher hardness/stiffness (e.g., unhydrated particles) display better abrasion resistance than those with lower hardness/stiffness (e.g., hydration products). Compared to HPC pastes, the scratch depth and residual scratch depth of UHPC pastes were reduced by 35 % and 38 %, respectively (Fig. 11(c and d)). This is because of the generation of high-stiffness hydrated phase and the existence of a considerable quantity of unhydrated cement particles in the UHPC, it exhibits superior abrasion resistance. Moreover, Du et al. [113] discovered that the incorporation of 0.01–0.1 % GO, especially at 0.1 %, could remarkably reduce the average scratch depth and enhance the abrasion resistance of concrete. It may be because the nucleation effect of GO enhances the hydration degree of cement, which strengthens the microstructure density and crack resistance.

To strengthen the wear resistance of concrete against debris flows, Wu et al. [38] studied the effect of different modifications methods (polyurea waterproofing adhesive (PUA), iron sheet (IS), polyurethane waterproof coating (PUR), and rubber) on the wear resistance of concrete by nanoscratch testing. The hard surface modifications (PUA and IS) considerably reduced the abrasion ratio of concrete, resulting in lower roughness after abrasion due to their superior scratch hardness and scratch resistance. Specifically, compared to ordinary concrete, the wear ratio for PUA and IS specimens was reduced by 75 % and 81 %, respectively. In contrast, the

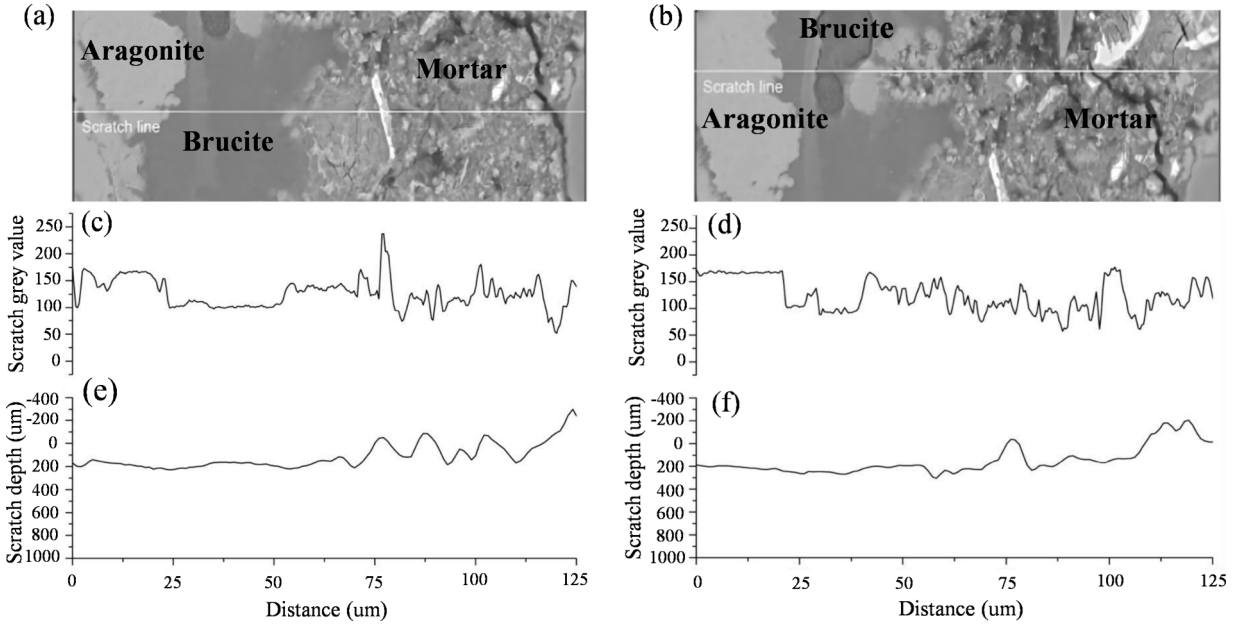

Fig. 10. Concrete immersed in seawater, (a and b) BSE images of the scratched positions; (c and d) the grey level distributions along the scratching path; and (e and f) corresponding scratching depth [72] (The copyright has been granted permission by the corresponding author).

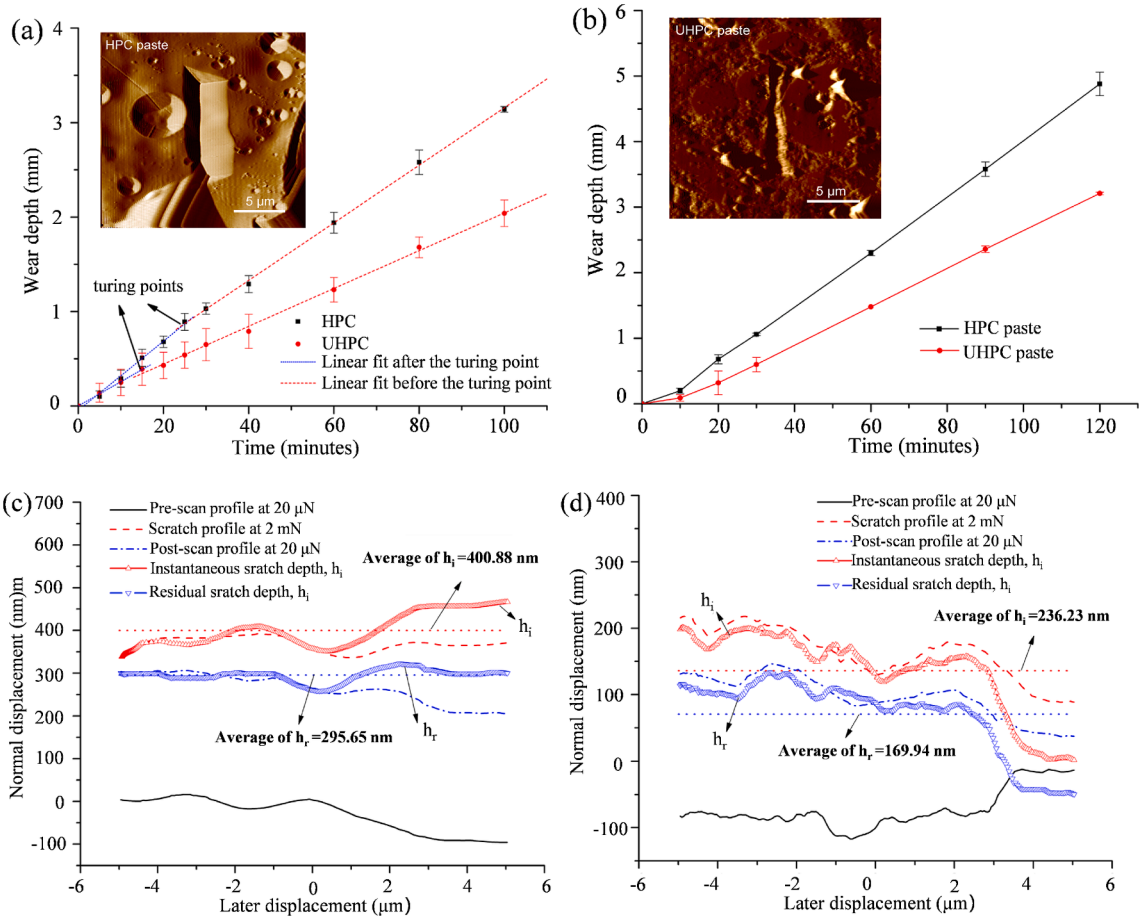

Fig. 11. Wear depth with time and scratch profile, (a, c) HPC, and (b, d) UHPC (reproduced under license number 1537768 from Ref. [53]).

soft surface treatments (PUR and RB) failed to offer sufficient protection for the concrete against debris flow attack due to their lower penetration depth and scratch hardness. Akono et al. [73] investigated the influence of rubber on the friction characteristic of concrete applied on the railway using nanoscratch testing. The findings revealed that incorporating 5 % rubber powder resulted in an approximately 10 % increase in the COF of the concrete, along with a slight enhancement in scratch hardness. This improvement contributes to enhancing the friction stability of concrete utilized in railway applications.

Barbhuiya et al. [91] employed nanoscratch and SEM methods to investigate the nanomechanical characteristics of cement pastes reinforced with short multi-walled carbon nanotubes (MWCNTs). The results showed that the MWCNTs-reinforced cement pastes has a smaller scratch penetration depth, compared to plain cement pastes. This is because of the role of MWCNTs as reinforcing components in the cement pastes, which enhances the resistance of the cement pastes to penetration. In addition, MWCNT-reinforced paste showed better abrasion resistance, with higher COF values and higher lateral forces obtained in the scratch test. Similar results were confirmed by the study of carbon nanofibers (CNFs)-reinforced cement composites [68]. Karimzadeh and Ayatollahi [126] also compared the effect of preparation methods on the abrasion resistance of cement pastes based on residual scratch depths derived from nanoscratch testing. The results showed that the average residual depth for cement mixed in air was 80 nm, while for the vacuum-mixed cement was 45 nm, which indicated that the vacuum-mixed cement pastes process had better abrasion resistance compared to that mixed in air. This is mainly attributed to cement paste produced by the vacuum mixing method having significantly lower porosity, which increased the connection between the polymer chains in cement paste, thus increasing the stiffness of cement pastes.

5.3. Interface properties

The interface phase exhibits extremely heterogeneous and is regarded to be the weakest component of CBM. Compared to the nanoindentation testing, the nanoscratch allows for continuous measurement of CBMs to acquire more comprehensive and reliable nanomechanical properties information, which is characterized by a wide testing range and high testing precision. As the scratch probe is moved to different phases, the nanoscratch parameters (e.g., depth of penetration, COF, and fracture toughness) change accordingly, which allows characterizing the interface between two phases in CBMs. Therefore, in addition to identifying the individual phases of the CBMs, the nanomechanical properties of the interface and fracture properties can be effectively obtained during scratch testing, as

shown in Table 3. Moreover, in addition to the ITZ between aggregate and cement matrix, some exquisite studies such as the interface between cement particles and cement pastes can also be carried out using nanoscratch testing.

5.3.1. Interface between unhydrated particles and matrix

Mao et al. [58] studied the properties of the interface between C-S-H gels and unhydrated particles in cement pastes at different w/c ratios and curing ages using nanoscratch testing. The distribution of different phases was identified by the variations of nanoscratch parameters (e.g., scratch depth, COF, and ERR). Then the width of the interface between the unhydrated particles and the C-S-H gels was determined though the sigmoidal curve fitting method. They found that the interface width between the unhydrated particles and the C-S-H gels ranged from 1 to 4 μm, which is mainly composed of HD C-S-H, and the HD C-S-H content increased as curing age while showing minimal sensitivity to w/c ratio. On this basis, Xu et al. [36] studied the interface properties between unhydrated particles and C-S-H gels of nanoSiO_2-modified cement pastes using nanoscratch tests. An improved sigmoidal curve fitting approach was mainly used to quantify the interface width by the COF value obtained from the nanoscratch testing. A tangent is drawn by fitting the inflection point of the curve and the baseline is extended to produce two intersections, the width between which is the average width of the interface (Fig. 12(a)). Because of the significant variation in COF values for different phases, the COF value is an effective method for calculating the interface width of CBMs [128,129]. The results revealed that the average interface width between the unhydrated particles and the C-S-H gels were about 200 nm, which was insensitive to the incorporation of nanoSiO_2. However, the COF values of the interface were remarkably reduced by incorporating nanoSiO_2 (Fig. 12(b)), which was attributed to the fact that the adhesion friction was reduced, because the incorporation of nanoSiO_2 had a densification effect on the interface. Xu et al [16]. also found that the incorporation of nanoSiO_2 had little impact on the width of interface, but had a remarkable effect on the nanomechanical characteristics of the interface through nanoindentation and modulus mapping testing.

In addition, due to the limitations of the polishing process, a completely smooth test surface cannot be achieved, which may result in errors in quantifying the interface width using the COF. Since there are large differences in the fracture toughness of interface, hydration product and clinker, Wei et al. [52] proposed a fracture toughness method for calculating width of interface and compared the differences of the interface width calculated by COF and fracture toughness methods (Fig. 13). The results indicated that the vertical loading rate and transverse scratch speed of the scratch test have a minor effect on the quantitative results of interface width, whether it is COF or fracture toughness method. The standard deviation of the interface width determined by the fracture toughness method was 0.0124 μm, while that determined though the COF method was 0.0151 μm. Because the influence of surface roughness is decreased, the standard deviation of interface width determined by the fracture toughness method is reduced by 17.9 % compared to the COF method. This indicated that the fracture toughness method is used to quantify interface widths with greater precision. Wei et al. [76] also investigated the interface properties of nanoSiO_2-modified cement pastes by fracture toughness method.

5.3.2. ITZ between fiber and matrix

The bond performance between the fibers and the matrix are crucial to the overall properties of the material, and nanoscratch has been used to research the nanomechanical characteristics and micro/nanostructure of fiber-reinforced CBMs. Hodzi et al. [128] compared the COF among the matrix, ITZ, and fiber obtained by nanoscratch testing, and the ITZ width was determined accordingly. Moreover, Hodzi et al. [128] reported that the nanoscratch testing seems to be a more sensitive method for detecting ITZ compared to nanoindentation because the impacted area of the pyramid probe on the material during nanoindentation is significantly smaller than the width detected in the experimental section. Barbhuiya et al. [68] investigated the ITZ nanomechanical characteristics of CNFs-reinforced cement paste by combining SEM tests and nanoscratch. The results showed that the CNFs were able to form strong ITZ bonding properties with the cement matrix, and the incorporation of CNFs has an influence of increasing the proportion of HD-CSH and decreasing the width of the ITZ.

Huang et al. [43] quantified the nanomechanical properties of the ITZ between carbon fibers (CF) and matrix in UHPC based on nanoscratch testing (Fig. 14). Among the four different CF-modification methods, the ITZ fracture toughness between the CF-modified by electrochemical oxidation technology (C4) and UHPC matrix was the highest, which was about 51 % higher than unmodified CF (C0). Furthermore, the ITZ width of the CF-modified with electrochemical oxidation technology (C4) to the matrix was approximately 0.6 μm, which was the smallest among all ITZs, only 46 % of that of the unmodified CFs (C0). This is because the oxidative modification of the CF makes the surface more hydrophilic, more hydration products are generated on the CF surface, and the ITZ becomes denser and improves fracture toughness. With the incorporation of silica fume (SF) at 10 %–20 % to the UHPC matrix, the fracture toughness of the ITZ between the unmodified CF and the matrix was increased by 12 %–18 %, and the ITZ width was reduced by 17 %–32 % compared to the specimen without SF. Attributed to SF having a much larger specific surface area than cement, which is more susceptible to agglomerate with CF and react with portlandite, leading to a reduction in the width of ITZ [36].

5.3.3. ITZ between aggregate and matrix

The ITZ between the aggregate and matrix is a critical factor affecting the performance and failure mechanism of CBMs [130]. Shu et al. [131] combined nanoscratch and SEM techniques to characterize the ITZ hardness and fracture toughness between aggregate and matrix in concrete. Based on the variation of scratch hardness along the scratch path, the aggregate/matrix interface was determined. The results indicated that the ITZ width of concrete was about 40 μm, and the scratch hardness of the ITZ was only about 75 % of the matrix, which further proves that the ITZ is the weakest phase in CBMs [132,133].

Many studies have shown that geopolymers exhibit better ITZ properties than OPC-based concrete [134,135]. Li et al. [74] investigated the nanomechanical characteristic of ITZ between aggregate and pastes in geopolymer composites with different silicon moduli ((SiO_2/Na_2O) of 1 and 1.5) by scratch and BSE techniques. The results showed that the ITZ properties of geopolymer specimens

Table 3
Application of scratch testing for phase identification and interface properties characterization.

Specimen types	Materials composition	Water/solid ratio	COF		Maximum penetration depth (nm)	K_C (MPa·m^{½})	Conclusion	Reference
Pure cement paste	Clinker	0.25			550		The interface width between C-S-H gels and cement particles is 1.74 μm for 7 d and 2.65 um for 28 d, respectively.	[58]
		0.30			900		The interface width between C-S-H gels and cement particles is 1.75 μm for 7 d and 3.30 um for 28 d, respectively.	
		0.30	Clinker Hydration products	0.26–0.30 0.35–0.38	1100		The volume fractions of clinker, hydration products, and pores are 32 %, 55 %, and 13 %, respectively.	[57]
		0.40	Clinker Hydration products	0.34–0.37 0.37–0.40	1200		The volume fractions of clinker, hydration products, and pores are 28 %, 44 %, and 28 %, respectively.	
			Clinker Interface	0.35 0.27	176 197			
	OPC	0.30	Clinker Hydration products Interface			1.44–1.68 0.71–1.09 0.60–0.65	The interface width between hydration products and cement particles is 0.9 μm; The fracture toughness of individual phases is between 0.60 and 1.88 MPa·m^{½}, with clinker exhibiting the highest value, followed by hydration products, and the interface phase is the lowest.	[52]
		0.40			12,500		The volume fractions of clinker, hydration products, and pores are 1.4 –16.7 %, 45.1 – 64.1 %, and 15 %, respectively.	[54]
		0.28	Clinker Hydration products Interface	0.20–0.24 0.34–0.36 0.20–0.34	176 466 197		The interface width between hydration products and unhydrated particles is 0.9 μm	[36]
Blend cement paste	OPC with 1 % nanoSiO$_2$	0.28	Clinker Hydration products Interface	0.16–0.26 0.33–0.31 0.11–0.21	172 443 154		The interface width between C-S-H gels and cement particles is 155 μm.	[36,127]
	OPC with 2 % nanoSiO$_2$	0.3	Clinker Hydration products Interface			1.59 ± 0.12 1.06 ± 0.16 1.06	The interface width between hydration products and cement particles is about 0.9 μm.	[76]
	OPC with 2 % carbon nanotubes		Clinker Hydration products Interface			1.61 ± 0.18 1.55 ± 0.17 1.55	The interface width between hydration products and cement particles is about 0.8 μm.	
	OPC with 15 % silica fume and 2 % carbon fiber	0.19	Hydration products ITZ carbon fiber	0.38–0.52 0.11–0.13 0.23–0.31	150 320	0.45–0.95 0.38–0.42 0.17–0.21	The ITZ width between hydration products and carbon fibers is about 1.4 μm.	[43]
Concrete	OPC with river sand as aggregates	0.5	Hydration products Aragonite and brucite		about 300 about 200		BSE imaging and nanoscratch technology have been combined to distinguish the phases of aragonite, brucite, and cement pastes.	[72]
Geopolymer	Low calcium FA with alkali solution and limestone as aggregates	0.33	Paste ITZ	0.31 ± 0.27 0.31 ± 0.30			The ITZ between aggregate and matrix process has strong nanomechanical properties (hardness and COF) which are similar to pastes.	[74]
		0.57					The hardness and elastic modulus of the top and bottom ITZs of a single aggregate were higher than those of the lateral ITZs.	[75]

*OPC: Ordinary Portland cement, ITZ: Interface transition zone, COF: Coefficient of friction, K_C: Fracture toughness. FA: fly ash.

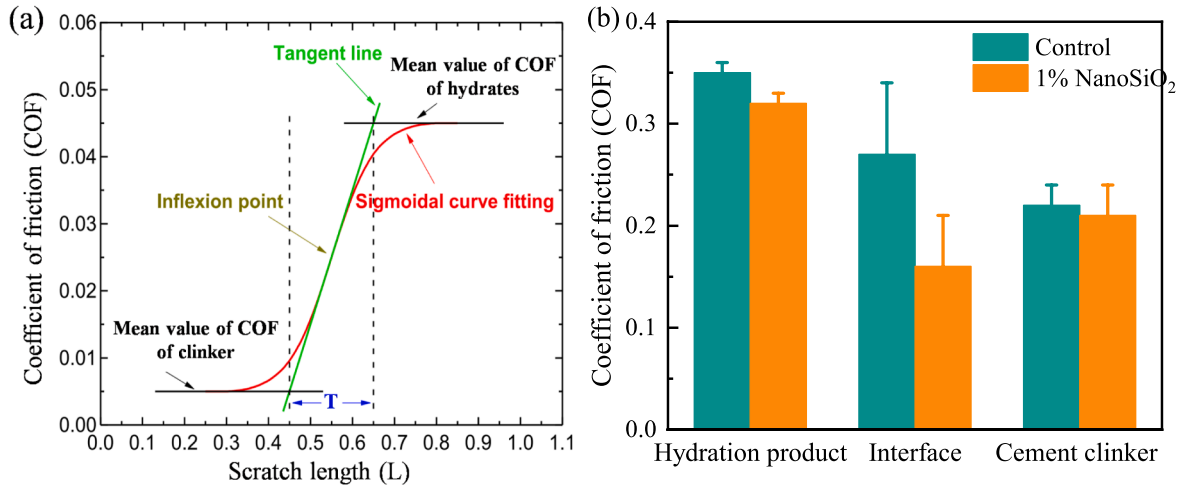

Fig. 12. Quantifying interface width of clinker to matrix in nanosilica modified cement pastes with w/c = 0.28, (a) the interface width determined using sigmoid fitting curve by COF and (b) COF of individual phase (data reused under license number 1538287 from Ref. [36]).

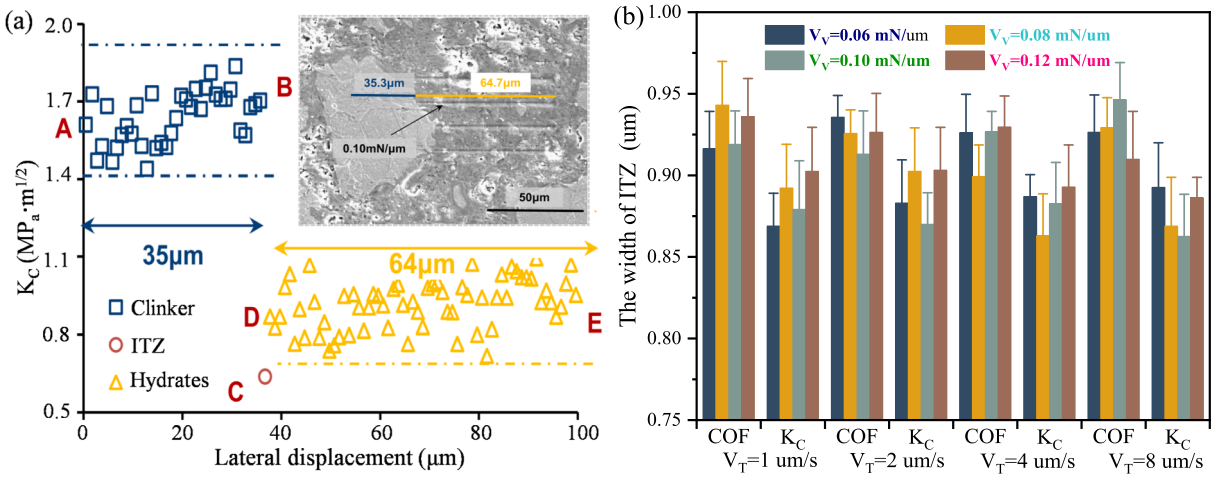

Fig. 13. Quantifying interface width of clinker to the matrix in cement paste with w/c = 0.3 (a) fracture toughness distribution and (b) test result of interface width (reproduced under license number 5893120286881 from Ref. [52]).

examined are not weaker than those of the pastes. For the silicon modulus of 1 and 1.5, the width of ITZ is determined to be about 30 and 40 μm, respectively. The ITZ in geopolymer with a silica modulus of 1.5 demonstrated similar hardness and COF to that observed in geopolymer pastes (Fig. 15(a)). However, the ITZs in the geopolymer with the silica modulus of 1 exhibited markedly higher scratch hardness but lower scratch friction coefficient than geopolymer pastes, which may because of the higher content of low-strength gels in the geopolymer pastes with silicon modulus of 1. In addition, Li et al. [74] proposed that, compared to the CL routine, the LIL routine that continuously traverses aggregate, ITZs, and geopolymer pastes has better potential in revealing the detailed variations of properties with increased distance from the aggregate. Luo et al. [75] studied the ITZ properties of various boundaries (top, bottom, and lateral boundaries) of individual aggregates in FA-based geopolymer concrete using nanoscratch and BSE image analysis. This study revealed that the distribution of the componential ratio of ITZs from various sides of the identical aggregate was not same, and the width of the ITZ was about 15, 35, and 30 μm at the top, bottom, and lateral, respectively, and the hardness of the top and bottom ITZs were higher than those of the lateral ITZs (Fig. 15(b). This may be attributed to the possibility of localized compaction during vibration process, which reinforces the microstructure of the top and bottom binders. In addition, FA accumulates on the top and bottom sides of ITZs because of vibration, while the increased small-sized particles with high reactivity can result in a higher reactive degree. This could further improve the nanomechanical properties at the top and bottom ITZs.

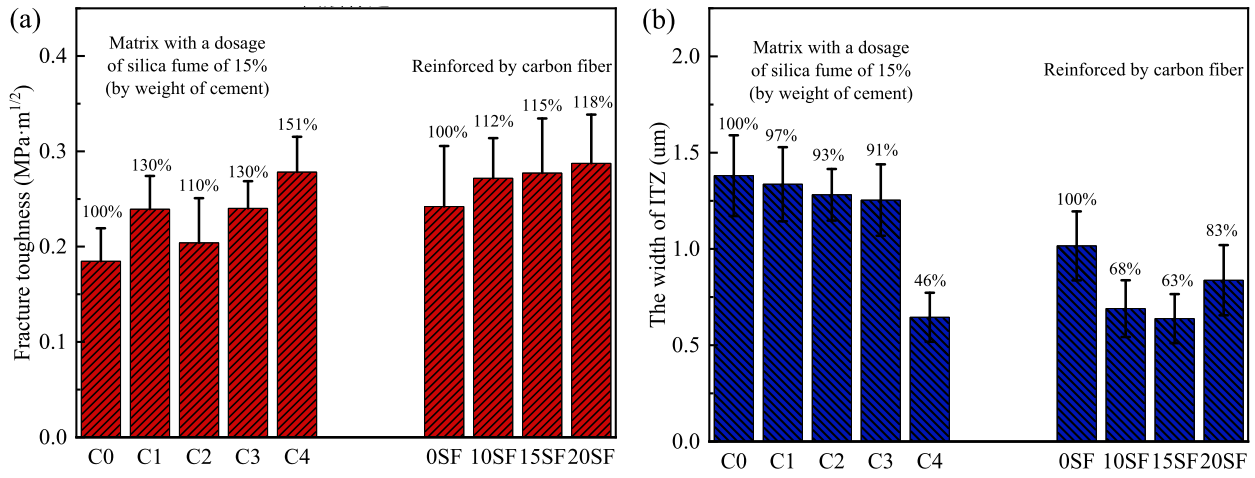

Fig. 14. The properties of ITZ between CF with various surface modifications (C0–C4) and the matrix with various SF contents (0SF–20%SF), (a) fracture toughness and (b) width of ITZ, C0: unmodified CF, C1: epoxy coating-modified CF, C2: gas oxidation-modified CF, C3: hydrophilic epoxy coating-modified CF, C4: electrochemical oxidation-modified CF (reproduced under license number 5893140854066 from Ref. [43]).

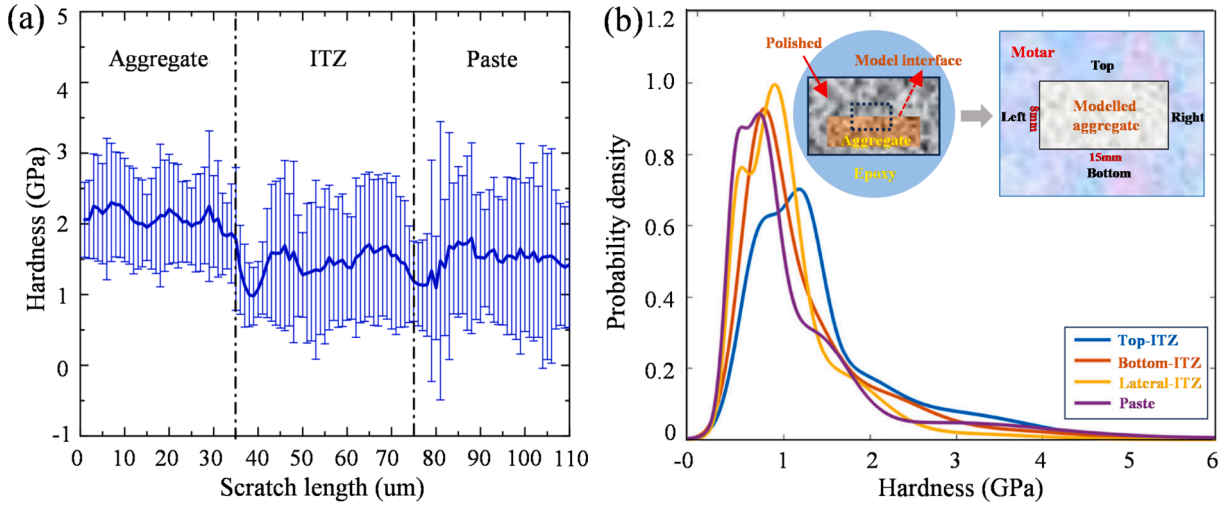

Fig. 15. (a) Hardness values of individual physical phases of geopolymer (silica modulus of 1.5) and (b) probability density distribution of different boundary hardness of aggregates (reproduced under license number 5893150064419 and 5893150378841 from Refs. [74;75]).

5.4. *Fracture properties*

The fracture properties of CBMs could be obtained by scratch testing, which reveals the failure mechanism of materials at the nanoscale. In scratch testing, localized plastic strains are generated when the scratch depth of the material is smaller than its characteristic length [136]. Therefore, it is essential to achieve the critical scratch depth in order to obtain representative fracture characteristics of the material [96,137]. The applied loads for fracture evaluation are under relatively high-level loads compared to mechanical and microstructure characterization, e.g., 7 [37], 10 [51], 30 [60,67,90] and 100 N [95], respectively. Hoover et al. [60] studied the functional correlations between hydration degree and fracture properties of cement pastes under different curing ages through nanoscratch testing with a 30 N load. The results showed that the evolution of fracture properties shows a natural logarithmic relationship with the hydration degree.

5.4.1. *Fracture properties of the matrix*

The distribution of fracture properties among individual phases needs to be characterized to reveal the transfer mechanism of the multi-scale characteristics of CBMs. Wei et al. [52] investigated the fracture properties of various phases in cement pastes by nanoscratch testing. Different phases can be easily identified from the probability density function curve of the fracture toughness (Fig. 16 (a)). The results showed that the fracture toughness of different phases in the cement pastes with a w/c ratio of 0.4 ranged from 0.60 to 1.88 MPa·m½. Unhydrated clinker exhibits the highest fracture toughness of 1.44–1.88 MPa·m½, followed by CH, HD C-S-H, LD C-S-H,

and interface (0.60–0.65 MPa·m½) (Fig. 16(b)). Interface exhibits the lowest fracture toughness among all the phases, which further proves that interface is the weakest phase determining the fracture properties of CBMs. It should be noted that, due to the minor differences in nanomechanical characteristics between C-S-H gels and the CH, distinguishing between them using scratch depths and COF methods in nanoscratch testing is challenging [138]. However, the CH phase can be identified by the fracture toughness distribution curve of individual phases because the average fracture toughness of CH is 1.06 MPa·$m^{1/2}$, which is 0.19 MPa·$m^{1/2}$ higher than that of the C-S-H gel. It indicates that the fracture toughness distribution method allows more precise phase identification for CBMs. Yao et al. [89,139] obtained similar results and pointed out that it is more accurate to identify the different phases along the scratch paths based on their elemental distributions using EDS analysis.

It is challenging to distinguish between CH and HD CSH using independent nanoscratch tests due to their similar fracture characteristics [52]. Němeček et al. [45] further quantified the primary components in the cement matrix, including inner hydration products, outer hydration products, and CH through the combination of nanoscratch testing and acoustic emission technique (Fig. 17). Due to the ordered microstructure of CH, it exhibits higher energy dissipation and a smaller propagation range during acoustic emission testing compared to C-S-H gels, allowing for its detection with greater sensitivity and stronger signal feedback. The resulted revealed the average fracture toughness of inner hydration products is 18.2 % higher than that of outer hydration products. Although the fracture toughness values of inner hydration products and CH are remarkably similar, they can be effectively distinguished by analyzing the intensity of acoustic emission signals.

5.4.2. *Effect of material composition on fracture properties*

Some studies indicated that the fracture properties can be effectively improved through optimizing the composition of CBMs. Krakowiak et al. [90] studied the influence of curing temperature and nanoSiO_2 content on the fracture properties of oil-well cement paste by nanoscratch testing. The results showed that the fracture toughness of oil-well cement initially increases, followed by a decrease as the curing temperature increases, and the SiO_2 addition can effectively prevent the decrease in fracture toughness. However, Lum and James [32] found that under different curing conditions, oil-well cement with identical w/c ratios exhibited virtually identical fracture toughness. Akono et al. [95] reported that the fracture toughness of cement pastes decreases with increasing w/c ratios, which was in agreement with the conventional theory that porosity increases and nanomechanical properties decrease with increasing w/c ratio. Akono [37] studied the effect of carbon-based nanomaterials on the fracture properties of cement pastes by nanoscratch test and BSE analysis methods. She showed that carbon-based nanomaterials can improve the fracture toughness of cement pastes, and the increase in fracture toughness of the CBMs is positively correlated with the mass fraction of carbon-based nanofillers (Fig. 18(a)), because the nanomaterials refine the pore structure, reduce porosity and enhance the microstructural compactness. Wei et al. [76] discovered that the addition of nanoSiO_2 into cement pastes increased the fracture toughness of the hydration product and the interface phase by 19 % and 56 %, respectively, while the incorporation of 0.08 % CNFs increased the fracture toughness by 74 % and 95 %, respectively. This means that the addition of nanoSiO_2 and CNF can both enhance the fracture toughness of cement pastes, but CNF is more effective (Fig. 18(b)). In addition, Akono [71] also reported that the incorporation of 1 % and 5 % nanoTiO_2 particles increased the fracture toughness of cement pastes by 3 % and 11 %, respectively.

Akono et al. [73] investigated the influence of crumb rubber on the friction and fracture properties of CBMs using scratch testing. They discovered that the average fracture toughness of the concrete increased by 38 % and 12 % with the addition of 5 % and 10 % crumb rubber particles, respectively (Fig. 18(c)). This was attributed to the inherent ductility of the rubber particles and the effect of the toughening mechanism, the fracture resistance of the concrete is enhanced by the addition of rubber particles [140]. It is commonly considered that the higher early strength would result in a higher brittleness of CBMs. Yao et al. [89] studied the effect of adding nano-seed materials on the nanomechanical properties of early-high strength cement paste and found that the addition of 1 % calcium-alumina −silicate-hydrate (C-A-S-H) nano-seeds increased the strength and fracture toughness of the early strength cement pastes

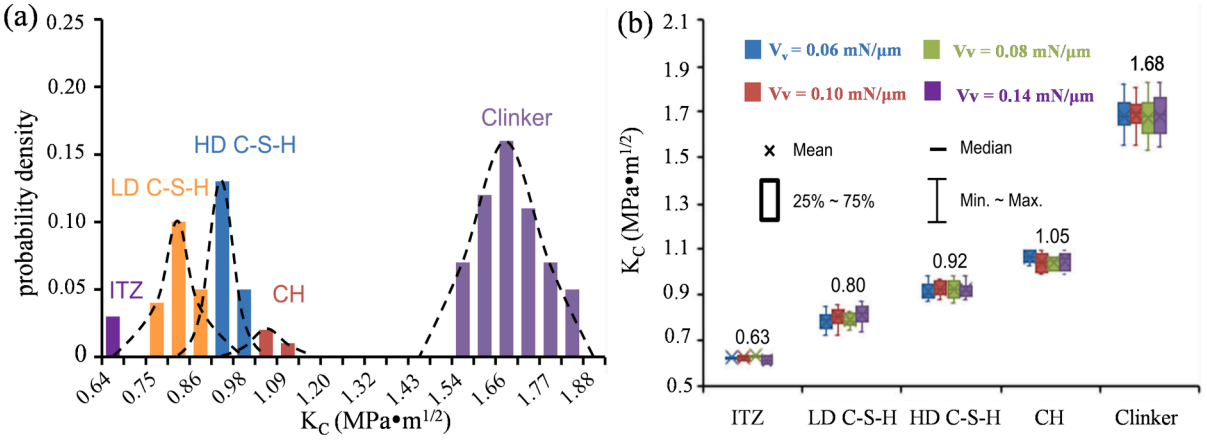

Fig. 16. Fracture toughness distribution in cement paste, (a) probability density curve, and (b) fracture toughness of various phases (reproduced under license number 5893120286881 from Ref. [52]).

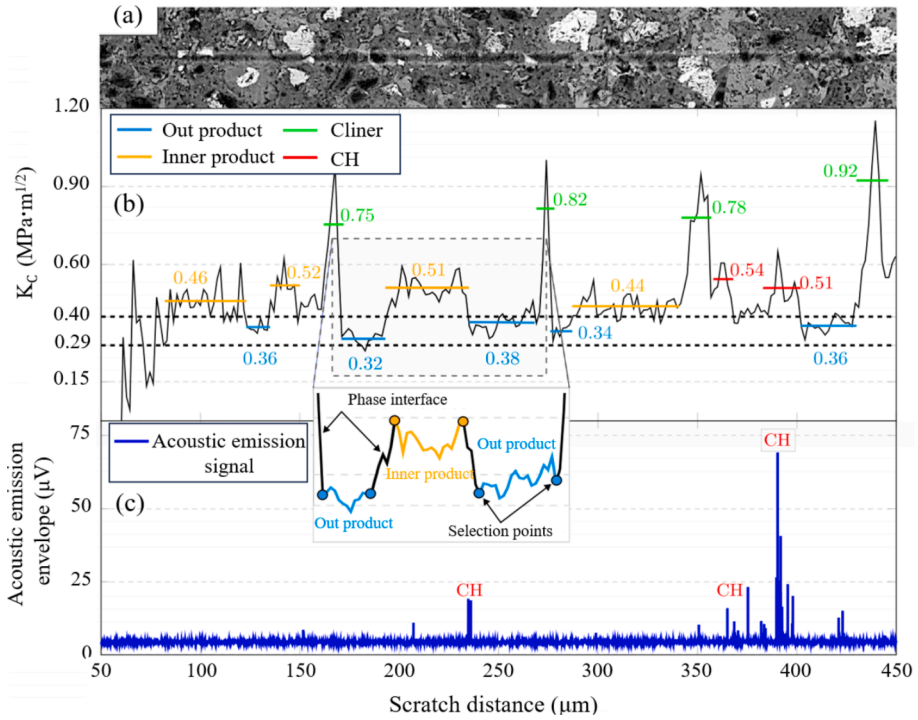

Fig. 17. Fracture toughness of various phases in cement matrix, (a) BSE imagine of the scratch positions, (b) the fracture toughness distributions along the scratch path and (c) corresponding acoustic emission envelope (reproduced under license number 5893150912292 from Ref. [45]).

by 78 % and 68 %, respectively. Chen and Akono [70] reported that the incorporation of 0.2 % and 0.5 % MWCNTs increased the fracture toughness of cement pastes by 9 % and 14 %, respectively (Fig. 18(d)). This is attributed to MWCNT inducing the conversion of LD C-S-H into HD C-S-H and reducing the width of the ITZ, thereby strengthening the cement paste. Johnson et al. [51] studied the fracture properties of the gel generated by the alkali-silica reaction in concrete at multiple scales and estimated the fracture energy of silicate gels. The results indicated that the fracture energy of alkali-silicate gels was one order of magnitude smaller than that of concrete. Anderson et al. [67] investigated the correlation between the fracture toughness and microstructure of calcium aluminate cement composites using scratch testing. They found that the failure of the cement paste transitions from brittle to ductile as the scratch depth increases. The fracture toughness of calcium aluminate cement composites decreased with the polymer-to-cement ratio increased. In addition, the high value of fracture toughness of calcium aluminate cement composites is attributed to the calcium aluminate phases and a highly filled non-porous particle nanostructure.

5.4.3. Effect of curing conditions on fracture toughness

Steam curing has been extensively as a means of enhancing the early performance of CBMs. Yao et al. [89] used nanoscratch testing to study the nanomechanical characteristics of cement pastes whose early-age properties are enhanced through steam curing. Yao et al. [89] discovered that the early strength and fracture toughness of cement pastes is enhanced by 63 % and 62 % respectively. The fracture toughness and fracture energy are some of the key characteristics to be studied in concrete subjected to frost attack. Kong et al. [40] studied the impact of the early freeze–thaw cycle on the fracture properties of various phases in cement pastes using nanoscratch testing. The results revealed that early freeze–thaw cycling reduced the fracture properties of hydration products and ITZ, while having no adverse impact on clinker. This phenomenon is primarily because frost attack increases the presence of LD C-S-H while simultaneously reducing the HD C-S-H and CH content. Wei et al. [76] investigated the fracture properties of nanofiller-reinforced cement composite at macroscales under freeze–thaw cycle conditions by nanoscratch testing and conventional three-point bending test methods. They found that freeze–thaw cycles hindered the increase of the fracture toughness of the interface and hydrate phases in cement pastes and nanoSiO_2 –reinforced pastes. The fracture toughness of the pastes was improved by the incorporation of nanomaterials (nanoSiO_2 and CNFs) under early freeze–thaw cycle conditions. However, early-age freeze–thaw cycling does not influence or diminish the fracture toughness of the interface and the hydrate phase when CNFs were incorporated (Fig. 19). The addition of both nanomaterials (the nanoSiO_2 and the CNFs) mitigated the reduction in fracture toughness due to the frost attack of cement pastes, but the CNFs were more effective, which was attributed to the bridging and nucleation effect of CNFs. Therefore, it is proposed to use CNFs to enhance the fracture toughness of CBMs that are susceptible to frost attack.

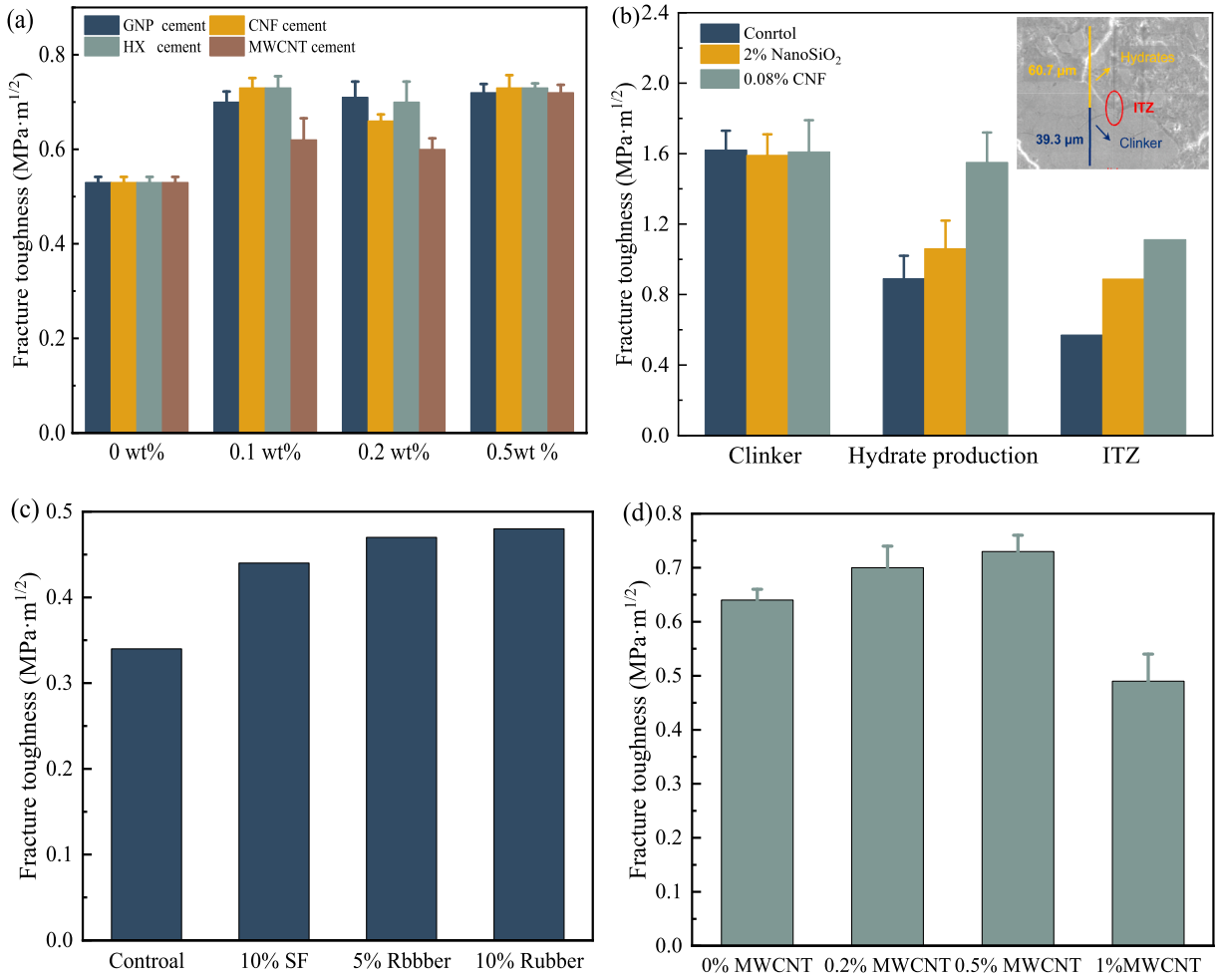

Fig. 18. Effect of (a) carbon-based nanomaterials, (b) nanoSiO$_2$ and CNF, (c) rubber, and (d) MWCNT on fracture toughness of CBMs, GNP: graphene nanoparticles, CNF: carbon nanofibers, HX: helical carbon nanotubes, and MWCNT: multi-walled carbon nanotubes (reproduced under Creative Commons license, license number 5893160784133, 5893161309975, and 5893170005555 from Refs. [37,76,73], and [70]).

6. Conclusions and outlook

Nanoscratch testing is characterized by continuous recording of results during the scratching process, which provides an abundant of data compared to discrete testing methods such as nanoindentation. The application of nanoscratch techniques has provided a crucial means for characterizations of CBMs properties at nanoscales, which provides a new opportunity for understanding the mechanism of the macroscopic performance evolution of CBMs. In this review, the specimen preparation, testing, and data analysis methods for nanoscratch testing have been summarized in detail. Then, combining nanoscratch and other multiple means to further investigate the multi-scale information of CBMs is discussed.

A flat and smooth specimen surface is essential to ensure the accuracy of nanomechanical characterization. Because of the multi-phase and multi-scale characteristics of CBMs, the surface roughness is relatively large. Therefore, the specimens should be carefully and meticulously prepared by cutting, grinding, and polishing to achieve uniformly flat and smooth testing surfaces, such as making it as flat and parallel to the substrate as possible by grinding, and slow polishing using oil-based polishing fluids with good particle size grading. As the surface roughness decreases, the variability of the scratch test results also decreases. Although the nanoscale roughness of cement specimen is difficult to eliminate, it should be controlled to an order of magnitude smaller than the scratch penetration depth (Typically less than 50 μm).

With the scratch load increases, the scratch depth gradually increases and tends to be stable. Too small scratch depth will cause the test results to be affected by the heterogeneity of each individual cement phase itself. However, too large scratch depth will cause the test results to be impacted by the interactions among various hydration phases in CBMs. Therefore, for multiphase heterogeneous materials such as CBMs, it is recommended that the maximum scratch depth should be kept in the range of 100–20000 nm

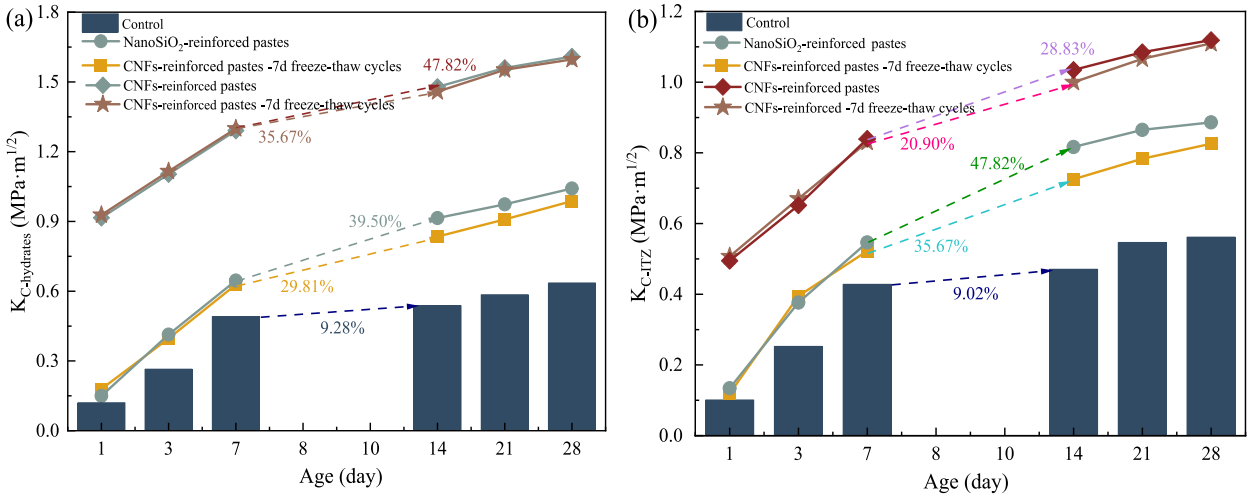

Fig. 19. The evolution of fracture toughness (a) cement pastes and (b) interface phase in cement pastes, NanoSiO$_2$ pastes, and CNFs pastes under non-frozen and frozen conditions. (data reused under license number 5893160784133 from Ref. [76]).

to improve the accuracy of the test. Moreover, reasonable scratch spacing (greater than 10 μm) is recommended to be chosen to prevent interactions among scratch points in the nanoscratch test.

The determination of the loading regime of nanoscratches largely depends on the purpose of the test and the type of CBMs being tested. The nanostructure of cement pastes, such as phase identification and interface width, is recommended to be characterized by CL routines under lower loads, which will hardly cause serious damage to the microstructure of the specimen. However, to obtain abrasion resistance and fracture properties for CBM, LIL routines at higher loads might be more effective, as this ensures that the concrete undergoes fracture failure damage rather than local plastic deformation. Moreover, the LIL routine also has the potential to identify more phases or to obtain more details about the nanoscale features of the CBMs.

Compared to nanoindentation, nanoscratch exhibits enhanced precision in characterizing relatively narrow interfaces. The width of interface between clinker and cement paste is typically less than 1 μm, which can be detected by the nanoscratch with its continuity measurement characteristics. However, due to the limitation of nanoindenter size, the spacing between adjacent indenter points is generally greater than 5 μm, so the indenter cannot accurately fall on the relatively small interface, which makes it difficult to accurately quantify the interface widths through nanoindentation. Meanwhile, an ITZ width of less than 5 μm between fibers and matrix in UHPC can also be accurately quantified using nanoscratch test rather than nanoindentation.

A large number of characteristic parameters such as scratch hardness, coefficient of friction, and fracture toughness, can be derived from the analysis of the scratch profile, which in turn able to be fitted and deconvolution analyzed by the probability density function (PDF) or cumulative distribution function (CDF) to determine the nanomechanical properties and volume fractions of various phases in CBM. In addition, the combination of the nanoscratch technology with various advanced testing methods such as BSE image analysis, nanoindentation will contribute to the further improve the accuracy of phase identification.

Although plenty of meaningful results had already been achieved in the research field of scratch testing. However, to improve the applicability of nanoscratch testing in multiple fields and the reliability of test results, the following aspects of efforts need to be resolved further:

(1) The process of specimen preparation should be further optimized to minimize both specimen disturbance and surface roughness. Therefore, a more reliable and standardized specimen preparation program needs to be established, and the influence of test conditions on nanomechanical properties testing should be taken into consideration so that the test results can be corrected accordingly. In addition, since surface roughness measurements exhibit non-negligible variations, the RMS method is highly dependent on the scan size. Potentially more accurate surface roughness quantification methods such as statistical analysis of curvature or surface slope need to be further demonstrated and developed.

(2) The phase identification is challenging. Previously, the type of phase was determined by characteristic parameters such as scratch hardness, COF, or fracture toughness. However, for special cement systems, such as magnesium-based cement, and alkali-activated material, these characteristic parameters fluctuate greatly or the parameters are unknown. Even the same phase in different systems may have different nanomechanical properties despite the same mineral composition. The nanomechanical characteristics parameters of a single mineral phase can be obtained by combined X-ray diffraction (XRD), BSE, and EDS from the perspective of a single mineral phase test, which provides a basis for identifying mixed phases in complex or unknown cement systems.

(3) Scratch profile is critical information for obtaining scratch characterization parameters and nanomechanical characteristics of CBMs. Topological and morphological analysis of the scratched area by image analysis techniques such as BSE and AFM, can help to further qualitatively determine the effects of deformation, failure mechanisms, and other factors on the variation of nanomechanical parameters during the scratching process. It promises to obtain the correlation among the physicochemical properties, packing

arrangement structure, and nanomechanical characteristics of hydration products at a smaller scale.

(4) OPC also produces phases such as sulfoaluminate and carbonate in very small quantity during the hydration process, which makes it difficult to form characteristic peaks during the deconvolution of the scratch test data. This may bring errors to the quantitative analysis of other phases. Therefore, it is essential to further optimize the analysis and screening of experimental data, minimize data dispersion, and ensure the reliability of the measured results by statistical mathematical means or modeling the correlation.

(5) Nanoscratch has shown excellent potential for the identification of interfaces between unhydrated cement particles and cement pastes, which provides the possibility to detect the reactivity of supplementary cementitious material particles. In addition, the continuous measurement nature of nanoscratch testing shows great potential for characterizing the interfacial bonding properties between the organic shells of encapsulated microorganisms and cement matrix.

(6) Nanoscratch exhibits high applicability in characterizing the nanoscale micorstructures and nanomechanical characteristics of CBMs. However, the transfer of nanoscale features to macroscopic properties and the establishment of multiscale models need to be further studied. Meanwhile, the large number of nanoscale results yielded by the nanoscratch tests need to be further combined with numerical simulations to predict the macroscopic properties of multiple types of CBMs.

CRediT authorship contribution statement

Zhi-hai He: Writing – review & editing, Funding acquisition, Conceptualization. **Wen-qiang Zhai:** Writing – original draft, Formal analysis, Data curation. **Jin-yan Shi:** Writing – review & editing, Conceptualization. **Cheng Du:** Conceptualization. **Ruo-miao Sun:** Conceptualization. **Çağlar Yalçınkaya:** Writing – review & editing. **Branko Šavija:** Writing – review & editing.

Declaration of competing interest

None.

Acknowledgement

The authors would like to acknowledge the Natural Science Foundation of Zhejiang Province (Grant No. LY20E020006).

Data availability

Data will be made available on request.

References

[1] Bernard O, Ulm F, Lemarchand E. A multiscale micromechanics-hydration model for the early-age elastic properties of cement-based materials. Cem Concr Res 2003;33(9):1293–309. https://doi.org/10.1016/S0008-8846(03)00039-5.
[2] Li L, Khan M, Bai C, Shi K. Uniaxial Tensile Behavior, Flexural Properties, Empirical Calculation and Microstructure of Multi-Scale Fiber Reinforced Cement-Based Material at Elevated Temperature. Materials 2021;14(8):1827. https://doi.org/10.3390/ma14081827.
[3] Constantinides G, Ulm F. The effect of two types of C-S-H on the elasticity of cement-based materials: Results from nanoindentation and micromechanical modeling. Cem Concr Res 2004;34(1):67–80. https://doi.org/10.1016/S0008-8846(03)00230-8.
[4] Lorenzoni R, Curosu I, Paciornik S, Mechtcherine V, Oppermann M, Silva F. Semantic segmentation of the micro-structure of strain-hardening cement-based composites (SHCC) by applying deep learning on micro-computed tomography scans. Cem Concr Compos 2020;108:103551. https://doi.org/10.1016/j.cemconcomp.2020.103551.
[5] Lee KM, Park JH. A numerical model for elastic modulus of concrete considering interfacial transition zone. Cem Concr Res 2008;38(3):396–402. https://doi.org/10.1016/j.cemconres.2007.09.019.
[6] Zhang H, Xu Y, Gan Y, Chang Z, Schlangen E, Šavija B. Microstructure informed micromechanical modelling of hydrated cement paste: Techniques and challenges. Constr Build Mater 2020;251:118983. https://doi.org/10.1016/j.conbuildmat.2020.118983.
[7] Constantinides G, Ulm F. The nanogranular nature of C–S–H. J Mech Phys Solids 2007;55(1):64–90. https://doi.org/10.1016/j.jmps.2006.06.003.
[8] Trtik P, Kaufmann J, Volz U. On the use of peak-force tapping atomic force microscopy for quantification of the local elastic modulus in hardened cement paste. Cem Concr Res 2012;42(1):215–21. https://doi.org/10.1016/j.cemconres.2011.08.009.
[9] Wei Y, Wu Z, Yao X, Gao X. Quantifying effect of later curing on pores of paste subject to early-age freeze-thaw cycles by different techniques. J Mater Civ Eng 2019;31(8):04019153.
[10] Vandamme M, Ulm F, Fonollosa P. Nanogranular packing of C–S–H at substochiometric conditions. Cem Concr Res 2010;40(1):14–26. https://doi.org/10.1016/j.cemconres.2009.09.017.
[11] P. Mondal. Nanomechanical Properties of Cementitious Materials, Northwestern University, 2008.
[12] Zanjani Zadeh V, Bobko CP. Nano-mechanical properties of internally cured kenaf fiber reinforced concrete using nanoindentation. Cem Concr Compos 2014;52:9–17. https://doi.org/10.1016/j.cemconcomp.2014.04.002.
[13] Liang M, He S, Gan Y, Zhang H, Chang Z, Schlangen E, et al. Predicting micromechanical properties of cement paste from backscattered electron (BSE) images by computer vision. Mater Des 2023;229:111905. https://doi.org/10.1016/j.matdes.2023.111905.
[14] Krakowiak KJ, Wilson W, James S, Musso S, Ulm F. Inference of the phase-to-mechanical property link via coupled X-ray spectrometry and indentation analysis: Application to cement-based materials. Cem Concr Res 2015;67:271–85. https://doi.org/10.1016/j.cemconres.2014.09.001.
[15] Davydov D, Jirásek M, Kopecký L. Critical aspects of nano-indentation technique in application to hardened cement paste. Cem Concr Res 2011;41(1):20–9. https://doi.org/10.1016/j.cemconres.2010.09.001.
[16] Xu J, Corr DJ, Shah SP. Nanomechanical investigation of the effects of nanoSiO2 on C–S–H gel/cement grain interfaces. Cem Concr Compos 2015;61:7–17. https://doi.org/10.1016/j.cemconcomp.2015.04.011.
[17] Gan Y, Zhang H, Liang M, Zhang Y, Schlangen E, van Breugel K, et al. Flexural strength and fatigue properties of interfacial transition zone at the microscale. Cem Concr Compos 2022;133:104717. https://doi.org/10.1016/j.cemconcomp.2022.104717.
[18] Beake BD, Vishnyakov VM, Harris AJ. Nano-scratch testing of (Ti,Fe)Nx thin films on silicon. Surf Coat Technol 2017;309:671–9. https://doi.org/10.1016/j.surfcoat.2016.11.024.

[19] Huang L, Lu J, Xu K. Elasto-plastic deformation and fracture mechanism of a diamond-like carbon film deposited on a Ti–6Al–4V substrate in nano-scratch test. Thin Solid Films 2004;466(1–2):175–82. https://doi.org/10.1016/j.tsf.2004.03.026.
[20] Harfouche MM, Alidokht SA, Islas Encalada A, Mungala VNV, Chromik RR, Moreau C, Sharifi N, Stoyanov P, Makowiec ME. Scratch Adhesion Testing of Thick HVOF Thermal Sprayed Coatings. J. Therm. Spray Technol. 2024;33(4):1158–66. https://doi.org/10.1007/s11666-024-01741-3.
[21] Li Y, Zhang L, Li C. Highly transparent and scratch resistant polysiloxane coatings containing silica nanoparticles. J Colloid Interface Sci 2020;559:273–81. https://doi.org/10.1016/j.jcis.2019.09.031.
[22] Bull SJ, Berasetegui EG. An overview of the potential of quantitative coating adhesion measurement by scratch testing. Tribol Int 2006;39(2):99–114. https://doi.org/10.1016/j.triboint.2005.04.013.
[23] Lin Y, Wu C, Wu B, Zhang G. Rapid synthesis of organosilicon oxide thin films and post-curing for enhanced scratch and corrosion resistance of aluminum alloy. Vacuum 2024;221:112879. https://doi.org/10.1016/j.vacuum.2023.112879.
[24] Sun Z, Espinoza DN, Balhoff MT, Dewers TA. Discrete Element Modeling of Micro-scratch Tests: Investigation of Mechanisms of CO2 Alteration in Reservoir Rocks. Rock Mech Rock Eng 2017;50(12):3337–48. https://doi.org/10.1007/s00603-017-1306-z.
[25] Li Z, Zhang F, Luo X, Cai Y. Fundamental understanding of the deformation mechanism and corresponding behavior of RB-SiC ceramics subjected to nano-scratch in ambient temperature. Appl Surf Sci 2019;469:674–83. https://doi.org/10.1016/j.apsusc.2018.11.090.
[26] Comakli R, Aldalahali AMJ. Effect of water saturation on Cerchar abrasivity index (CAI) of clay-rich rocks at different scratch lengths. Wear 2024;538–539: 205187. https://doi.org/10.1016/j.wear.2023.205187.
[27] Jeyaprakash N, Kumar MS, Yang C. Enhanced nano-level mechanical responses on additively manufactured Cu-Cr-Zr copper alloy containing Cu2O nano precipitates. J Alloy Compd 2023;930:167425. https://doi.org/10.1016/j.jallcom.2022.167425.
[28] Liu J, Jiang H, Cheng Q, Wang C. Investigation of nano-scale scratch and stick-slip behaviors of polycarbonate using atomic force microscopy. Tribol Int 2018; 125:59–65. https://doi.org/10.1016/j.triboint.2018.04.024.
[29] Kovalets NP, Kozhina EP, Razumovskaya IV, Arzhanov AI, Naumov V. Scratching of metallized polymer films by Vickers indenter as a method for controlled production of SERS-active metasurfaces. J Lumin 2024;275:120803. https://doi.org/10.1016/j.jlumin.2024.120803.
[30] Xu J, Corr DJ, Shah SP. Nanomechanical properties of C-S-H gel/cement grain interface by using nanoindentation and modulus mapping. Journal of Zhejiang University A Science 2015;16(1):38–46. https://doi.org/10.1631/jzus.A1400166.
[31] Fett T, Kounga Njiwa AB, Rödel J. Crack opening displacements of Vickers indentation cracks. Eng. Fract. Mech. 2005;72(5):647–59. https://doi.org/10.1016/j.engfracmech.2004.07.003.
[32] Ulm F, James S. The scratch test for strength and fracture toughness determination of oil well cements cured at high temperature and pressure. Cem Concr Res 2011;41(9):942–6. https://doi.org/10.1016/j.cemconres.2011.04.014.
[33] Bard R, Ulm F. Scratch hardness-strength solutions for cohesive-frictional materials. Int J Numer Anal Methods Geomech 2012;36(3):307–26. https://doi.org/10.1002/nag.1008.
[34] Beake BD, Harris AJ, Liskiewicz TW. Review of recent progress in nanoscratch testing. Tribol Mater Surf Interfaces 2013;7(2):87–96. https://doi.org/10.1179/1751584X13Y.0000000037.
[35] Kim HH, Cho SH, Kang CG. Evaluation of microstructure and mechanical properties by using nano/micro-indentation and nanoscratch during aging treatment of rheo-forged Al 6061 alloy. Mater Sci Eng A 2008;485(1–2):272–81. https://doi.org/10.1016/j.msea.2007.07.085.
[36] Xu J, Corr DJ, Shah SP. Nanoscratch Study of the Modification Effects of NanoSiO 2 on C— S— H Gel/Cement Grain Interfaces. J Mater Civ Eng 2017;29(9): 04017093.
[37] Akono A. Fracture toughness of one- and two-dimensional nanoreinforced cement via scratch testing. Phil Trans R Soc A 2021;379(2203):20200288. https://doi.org/10.6084/m9.figshare.
[38] Wu F, Chen X, Chen J. Abrasion resistance enhancement of concrete using surface treatment methods. Tribol Int 2023;179:108180. https://doi.org/10.1016/j.triboint.2022.108180.
[39] Němeček J, Šmilauer V, Čtvrtlík R. In: Fracture of cement hydrates determined from micro-scratching tests and their modeling. CRC Press; 2022. p. 59–65.
[40] Kong W, Wei Y, Wang Y, Sha A. Development of micro and macro fracture properties of cementitious materials exposed to freeze-thaw environment at early ages. Constr Build Mater 2021;271:121502. https://doi.org/10.1016/j.conbuildmat.2020.121502.
[41] Du S, Jiang Y, Zhong J, Ge Y, Shi X. Surface abrasion resistance of high-volume fly ash concrete modified by graphene oxide: Macro- and micro-perspectives. Constr Build Mater 2020;237:117686. https://doi.org/10.1016/j.conbuildmat.2019.117686.
[42] Bagheri M, Lothenbach B, Shakoorioskooie M, Leemann A, Scrivener K. Use of scratch tracking method to study the dissolution of alpine aggregates subject to alkali silica reaction. Cem Concr Compos 2021;124:104260. https://doi.org/10.1016/j.cemconcomp.2021.104260.
[43] Huang H, Peng C, Luo J, Sun T, Deng T, Hu J, He Z, Wei J, Yu Q, Anvarovna KG, Davlatali Ugli NA. Micromechanical properties of interfacial transition zone between carbon fibers and UHPC matrix based on nano-scratching tests. Cement and Concrete Composites. 2023;139:105014. https://doi.org/10.1016/j.cemconcomp.2023.105014.
[44] Etminani MA, Sharif F. Effect of fiber nano-scratch on macro strain hardening behavior in engineered cementitious composites. Physica. B, Condensed Matter 2018;545:442–51. https://doi.org/10.1016/j.physb.2018.03.006.
[45] Němeček J, Čtvrtlík R, Václavek L, Němeček J. Fracture toughness of cement paste constituents assessed by micro-scratching correlated with acoustic emission. Cem Concr Res 2024;185:107623. https://doi.org/10.1016/j.cemconres.2024.107623.
[46] Kim J, Lee J, Lee Y, Jang J, Kwon D. Surface roughness effect in instrumented indentation: A simple contact depth model and its verification. J Mater Res 2006; 21(12):2975–8. https://doi.org/10.1557/jmr.2006.0370.
[47] Donnelly E, Baker SP, Boskey AL, van der Meulen MC. Effects of surface roughness and maximum load on the mechanical properties of cancellous bone measured by nanoindentation. J Biomed Mater Res Part A 2006;77(2):426–35. https://doi.org/10.1002/jbm.a.30633.
[48] Miller M, Bobko C, Vandamme M, Ulm F. Surface roughness criteria for cement paste nanoindentation. Cem Concr Res 2008;38(4):467–76. https://doi.org/10.1016/j.cemconres.2007.11.014.
[49] Chen L, Ahadi A, Zhou J, Ståhl J. Modeling Effect of Surface Roughness on Nanoindentation Tests. Procedia CIRP 2013;8:334–9. https://doi.org/10.1016/j.procir.2013.06.112.
[50] Trtik P, Dual J, Muench B, Holzer L. Limitation in obtainable surface roughness of hardened cement paste: 'virtual' topographic experiment based on focussed ion beam nanotomography datasets. J Microsc (Oxford) 2008;232(2):200–6. https://doi.org/10.1111/j.1365-2818.2008.02090.x.
[51] Johnson CV, Chen J, Hasparyk NP, Monteiro PJM, Akono AT. Fracture properties of the alkali silicate gel using microscopic scratch testing. Cem Concr Compos 2017;79:71–5. https://doi.org/10.1016/j.cemconcomp.2017.01.012.
[52] Wei Y, Kong W, Wang Y, Sha A. Multifunctional application of nanoscratch technique to characterize cementitious materials. Cem Concr Res 2021;140: 106318. https://doi.org/10.1016/j.cemconres.2020.106318.
[53] Zhao S, Van Dam E, Lange D, Sun W. Abrasion resistance and nanoscratch behavior of an ultra-high performance concrete. J Mater Civ Eng 2017;29(2): 04016212. https://doi.org/10.1061/(asce)mt.1943-5533.0001744.
[54] Liu J, Zeng Q, Xu S. Is scratch test proper to characterize microstructure and mechanical properties of cement-based materials? The effects of loading level and routine. Cem Concr Res 2020;133:106072. https://doi.org/10.1016/j.cemconres.2020.106072.
[55] Thomas S, Bongiovanni C, Nutt SR. In situ estimation of through-thickness resin flow using ultrasound. Compos Sci Technol 2008;68(15):3093–8. https://doi.org/10.1016/j.compscitech.2008.07.012.
[56] Khedmati M, Kim Y, Turner JA, Alanazi H, Nguyen C. An integrated microstructural-nanomechanical-chemical approach to examine material-specific characteristics of cementitious interphase regions. Mater Charact 2018;138:154–64. https://doi.org/10.1016/j.matchar.2018.01.045.
[57] Xu J, Yao W. Nano-scratch as a new tool for assessing the nano-tribological behavior of cement composite. Mater Struct 2011;44(9):1703–11. https://doi.org/10.1617/s11527-011-9728-7.

[58] Mao Y, Yao W, Xu J. Study on the Unhydrated Cement Grain/C-S-H Gel Interface in Cement Paste by Use of Nano-Scratch Technique. Key Eng Mater 2013;539:84–8. https://doi.org/10.4028/www.scientific.net/KEM.539.84.

[59] Konsta-Gdoutos MS, Metaxa ZS, Shah SP. Multi-scale mechanical and fracture characteristics and early-age strain capacity of high performance carbon nanotube/cement nanocomposites. Cem Concr Compos 2010;32(2):110–5. https://doi.org/10.1016/j.cemconcomp.2009.10.007.

[60] Hoover CG, Ulm F. Experimental chemo-mechanics of early-age fracture properties of cement paste. Cem Concr Res 2015;75:42–52. https://doi.org/10.1016/j.cemconres.2015.04.004.

[61] Liu H, Ren X, Li J. Indentation tests based multi-scale random media modeling of concrete. Constr Build Mater 2018;168:209–20. https://doi.org/10.1016/j.conbuildmat.2018.02.050.

[62] Lomboy GR, Wang K, Sundararajan S. Nanoscale characterization of cementitious materials. ACI Mater. J. 2008;105(2):107. https://doi.org/10.1007/978-3-319-17088-6_5.

[63] Sakulich AR, Li VC. Nanoscale characterization of engineered cementitious composites (ECC). Cem Concr Res 2011;41(2):169–75. https://doi.org/10.1016/j.cemconres.2010.11.001.

[64] Hu C, Xu B, Ma H, Chen B, Li Z. Micromechanical investigation of magnesium oxychloride cement paste. Constr Build Mater 2016;105:496–502. https://doi.org/10.1016/j.conbuildmat.2015.12.182.

[65] Mondal P, Shah SP, Marks L. A reliable technique to determine the local mechanical properties at the nanoscale for cementitious materials. Cem Concr Res 2007;37(10):1440–4. https://doi.org/10.1016/j.cemconres.2007.07.001.

[66] Zhao S, Sun W. Nano-mechanical behavior of a green ultra-high performance concrete. Constr Build Mater 2014;63:150–60. https://doi.org/10.1016/j.conbuildmat.2014.04.029.

[67] Anderson K, Akono A. Microstructure–toughness relationships in calcium aluminate cement–polymer composites using instrumented scratch testing. J Mater Sci 2017;52(22):13120–32. https://doi.org/10.1007/s10853-017-1416-8.

[68] Barbhuiya S, Chow P. Nanoscaled Mechanical Properties of Cement Composites Reinforced with Carbon Nanofibers. Materials 2017;10(6):662. https://doi.org/10.3390/ma10060662.

[69] Lee H, Vimonsatit V, Chindaprasirt P. Mechanical and micromechanical properties of alkali activated fly-ash cement based on nano-indentation. Constr Build Mater 2016;107:95–102. https://doi.org/10.1016/j.conbuildmat.2015.12.013.

[70] Chen J, Akono A. Influence of multi-walled carbon nanotubes on the hydration products of ordinary Portland cement paste. Cem Concr Res 2020;137:106197. https://doi.org/10.1016/j.cemconres.2020.106197.

[71] Akono A. Effect of nano-TiO2 on C–S–H phase distribution within Portland cement paste. J Mater Sci 2020;55(25):11106–19. https://doi.org/10.1007/s10853-020-04847-5.

[72] Palin D, Thijssen A, Wiktor V, et al. ESEM-BSE coupled with rapid nano-scratching for micro-physicochemical analysis of marine exposed concrete[J]. EMABM 2015: Proceedings of the 15th Euroseminar on Microscopy Applied to Building Materials, Delft, The Netherlands, 17-19 June 2015 (2015).

[73] Akono A, Chen J, Kaewunruen S. Friction and fracture characteristics of engineered crumb-rubber concrete at microscopic lengthscale. Constr Build Mater 2018;175:735–45. https://doi.org/10.1016/j.conbuildmat.2018.04.141.

[74] Li W, Luo Z, Gan Y, Wang K, Shah SP. Nanoscratch on mechanical properties of interfacial transition zones (ITZs) in fly ash-based geopolymer composites. Compos Sci Technol 2021;214:109001. https://doi.org/10.1016/j.compscitech.2021.109001.

[75] Luo Z, Li W, Wang K, Shah SP, Sheng D. Nano/micromechanical characterisation and image analysis on the properties and heterogeneity of ITZs in geopolymer concrete. Cem Concr Res 2022;152:106677. https://doi.org/10.1016/j.cemconres.2021.106677.

[76] Wei Y, Kong W, Wang Y. Strengthening mechanism of fracture properties by nano materials for cementitious materials subject to early-age frost attack. Cem Concr Compos 2021;119:104025. https://doi.org/10.1016/j.cemconcomp.2021.104025.

[77] Akono A, Randall NX, Ulm F. Experimental determination of the fracture toughness via microscratch tests: Application to polymers, ceramics, and metals. J Mater Res 2012;27(2):485–93. https://doi.org/10.1557/jmr.2011.402.

[78] Němeček J. Creep effects in nanoindentation of hydrated phases of cement pastes. Mater Charact 2009;60(9):1028–34. https://doi.org/10.1016/j.matchar.2009.04.008.

[79] He Z, Han X, Zhang M, Yuan Q, Shi J, Zhang P. A novel development of green UHPC containing waste concrete powder derived from construction and demolition waste. Powder Technol 2022;398:117075.

[80] Kim JJ, Foley EM, Reda Taha MM. Nano-mechanical characterization of synthetic calcium–silicate–hydrate (C–S–H) with varying CaO/SiO2 mixture ratios. Cem Concr Compos 2013;36:65–70. https://doi.org/10.1016/j.cemconcomp.2012.10.001.

[81] Hu C, Li Z. Property investigation of individual phases in cementitious composites containing silica fume and fly ash. Cem Concr Compos 2015;57:17–26. https://doi.org/10.1016/j.cemconcomp.2014.11.011.

[82] Papatzani S, Paine K, Calabria-Holley J. A comprehensive review of the models on the nanostructure of calcium silicate hydrates. Constr Build Mater 2015;74:219–34. https://doi.org/10.1016/j.conbuildmat.2014.10.029.

[83] Fan D, Yang S. Mechanical properties of C-S-H globules and interfaces by molecular dynamics simulation. Constr Build Mater 2018;176:573–82. https://doi.org/10.1016/j.conbuildmat.2018.05.085.

[84] Xin H, Lin W, Fu J, Li W, Wang Z. Temperature Effects on Tensile and Compressive Mechanical Behaviors of C-S-H Structure via Atomic Simulation. J Nanomater 2017;2017:1–6. https://doi.org/10.1155/2017/8476258.

[85] Alizadeh R, Beaudoin JJ, Raki L. Viscoelastic nature of calcium silicate hydrate. Cem Concr Compos 2010;32(5):369–76. https://doi.org/10.1016/j.cemconcomp.2010.02.008.

[86] Delafargue A, Ulm F. Explicit approximations of the indentation modulus of elastically orthotropic solids for conical indenters. Int J Solids Struct 2004;41(26):7351–60. https://doi.org/10.1016/j.ijsolstr.2004.06.019.

[87] Ganneau FP, Constantinides G, Ulm FJ. Dual-indentation technique for the assessment of strength properties of cohesive-frictional materials. Int J Solids Struct 2006;43(6):1727–45. https://doi.org/10.1016/j.ijsolstr.2005.03.035.

[88] Xu J, Yao W. An Experimental Study of the Nano-Scratch Behavior of Cement Composite Material. Key Eng Mater 2011;492:47–54. https://doi.org/10.4028/www.scientific.net/KEM.492.47.

[89] Yao S, Zou F, Wang F, He Y, Hu S, Hu C. Revealing the micro-mechanical characteristics of high early strength cement pastes. Constr Build Mater 2022;342:128078. https://doi.org/10.1016/j.conbuildmat.2022.128078.

[90] Krakowiak KJ, Thomas JJ, Musso S, James S, Akono A, Ulm F. Nano-chemo-mechanical signature of conventional oil-well cement systems: Effects of elevated temperature and curing time. Cem Concr Res 2015;67:103–21. https://doi.org/10.1016/j.cemconres.2014.08.008.

[91] Barbhuiya S, Chow P. Nanoscale mechanical properties of cement paste reinforced with short carbon nanotubes. Proceedings of the Institution of Civil Engineers - Construction Materials 2019;172(2):63–70. https://doi.org/10.1680/jcoma.17.00025.

[92] Xu J, Corr DJ, Shah SP. Nanoscratch Study of the Modification Effects of NanoSiO2 on C—S—H Gel/Cement Grain Interfaces. J Mater Civ Eng 2017;29(9):04017093.

[93] Richardson IG. Tobermorite/jennite- and tobermorite/calcium hydroxide-based models for the structure of C-S-H: applicability to hardened pastes of tricalcium silicate, β-dicalcium silicate, Portland cement, and blends of Portland cement with blast-furnace slag, metakaolin, or silica fume. Cem Concr Res 2004;34(9):1733–77. https://doi.org/10.1016/j.cemconres.2004.05.034.

[94] Ulm F, Vandamme M, Jennings HM, Vanzo J, Bentivegna M, Krakowiak KJ, et al. Does microstructure matter for statistical nanoindentation techniques? Cem Concr Compos 2010;32(1):92–9. https://doi.org/10.1016/j.cemconcomp.2009.08.007.

[95] Akono AT. Energetic Size Effect Law at the Microscopic Scale: Application to Progressive-Load Scratch Testing. Journal of Nanomechanics and Micromechanics 2016;6(2):04016001.

[96] Akono A, Ulm F. Fracture scaling relations for scratch tests of axisymmetric shape. J Mech Phys Solids 2012;60(3):379–90. https://doi.org/10.1016/j.jmps.2011.12.009.

[97] Chen Y, Bakshi SR, Agarwal A. Correlation between nanoindentation and nanoscratch properties of carbon nanotube reinforced aluminum composite coatings. Surf Coat Technol 2010;204(16–17):2709–15. https://doi.org/10.1016/j.surfcoat.2010.02.024.
[98] Mulliah D, Christopher D, Kenny SD, Smith R. Nanoscratching of silver (100) with a diamond tip. Nucl Instrum Methods Phys Res, Sect B 2003;202:294–9. https://doi.org/10.1016/S0168-583X(02)01872-4.
[99] Chamani HR, Ayatollahi MR. The effect of Berkovich tip orientations on friction coefficient in nanoscratch testing of metals. Tribol Int 2016;103:25–36. https://doi.org/10.1016/j.triboint.2016.06.036.
[100] Xu N, Han W, Wang Y, Li J, Shan Z. Nanoscratching of copper surface by CeO2. Acta Mater 2017;124:343–50. https://doi.org/10.1016/j.actamat.2016.11.008.
[101] Zhao J, Zhang Q, Lu G, Chen D. A Peridynamic Approach for Nanoscratch Simulation of the Cement Mortar. In: IOP Conference Series: Materials Science and Engineering, Vol. 322, No. 4; 2018. p. 042004. https://doi.org/10.1088/1757-899X/322/4/042004.
[102] Akono A, Bouché GA. Rebuttal: Shallow and deep scratch tests as powerful alternatives to assess the fracture properties of quasi-brittle materials. Eng Fract Mech 2016;158:23–38. https://doi.org/10.1016/j.engfracmech.2016.02.010.
[103] Kimm J, Sander M, Pöhl F, Theisen W. Micromechanical characterization of hard phases by means of instrumented indentation and scratch testing. Materials Science & Engineering. A, Structural Materials: Properties, Microstructure and Processing 2019;768:138480. https://doi.org/10.1016/j.msea.2019.138480.
[104] Carreon AH, Funkenbusch PD. Material specific nanoscratch ploughing friction coefficient. Tribol Int 2018;126:363–75. https://doi.org/10.1016/j.triboint.2018.05.027.
[105] Gassilloud R. Mechanical Surface Nano-Patterning of Indium Phosphide and Silicon for Subsequent Electrochemical Processing. Friedrich-Alexander-Universitaet Erlangen-Nuernberg (Germany) 2006.
[106] Williams JA. Analytical models of scratch hardness. Tribol Int 1996;29(8):675–94. https://doi.org/10.1016/0301-679X(96)00014-X.
[107] Akono A, Ulm F. Scratch test model for the determination of fracture toughness. Eng Fract Mech 2011;78(2):334–42. https://doi.org/10.1016/j.engfracmech.2010.09.017.
[108] Lafaye S, Gauthier C, Schirrer R. Analyzing friction and scratch tests without in situ observation. Wear 2008;265(5–6):664–73. https://doi.org/10.1016/j.wear.2007.12.005.
[109] Sinha SK, Song T, Wan X, Tong Y. Scratch and normal hardness characteristics of polyamide 6/nano-clay composite. Wear 2009;266(7–8):814–21. https://doi.org/10.1016/j.wear.2008.12.010.
[110] Charitidis C, Panayiotatos Y, Logothetidis S. A quantitative study of the nano-scratch behavior of boron and carbon nitride films. Diam Relat Mat 2003;12(3):1088–92. https://doi.org/10.1016/S0925-9635(02)00268-6.
[111] Lee K, Marimuthu KP, Kim C, Lee H. Scratch-tip-size effect and change of friction coefficient in nano / micro scratch tests using XFEM. Tribol Int 2018;120:398–410. https://doi.org/10.1016/j.triboint.2018.01.003.
[112] Tariq Z, Murtaza M, Mahmoud M. Effects of Nanoclay and Silica Flour on the Mechanical Properties of Class G Cement. ACS Omega 2020;5(20):11643–54. https://doi.org/10.1021/acsomega.0c00943.
[113] Du S, Tang Z, Zhong J, Ge Y, Shi X. Effect of admixing graphene oxide on abrasion resistance of ordinary portland cement concrete. AIP Adv 2019;9(10):105110. https://doi.org/10.1063/1.5124388.
[114] Bucaille JL, Felder E, Hochstetter G. Mechanical analysis of the scratch test on elastic and perfectly plastic materials with the three-dimensional finite element modeling. Wear 2001;249(5):422–32. https://doi.org/10.1016/S0043-1648(01)00538-5.
[115] Beake BD, Ranganathan N. An investigation of the nanoindentation and nano/micro-tribological behaviour of monolayer, bilayer and trilayer coatings on cemented carbide. Mater Sci Eng A 2006;423(1–2):46–51. https://doi.org/10.1016/j.msea.2005.11.066.
[116] Akono AT, Ulm FJ. Microscopic toughness of viscous solids via scratching: from amorphous polymers to gas shale. Journal of Nanomechanics and Micromechanics 2017;7(3):4017009.
[117] Kabir P, Ulm F, Akono A. Rate-independent fracture toughness of gray and black kerogen-rich shales. Acta Geotech 2017;12(6):1207–27. https://doi.org/10.1007/s11440-017-0562-0.
[118] Akono A, Reis PM, Ulm F. Scratching as a fracture process: from butter to steel. Phys. Rev. Lett 2011;106(20):204302. https://doi.org/10.1103/PhysRevLett.106.204302.
[119] Lin J, Zhou Y. Can scratch tests give fracture toughness? Eng Fract Mech 2013;109:161–8. https://doi.org/10.1016/j.engfracmech.2013.06.002.
[120] Akono A, Ulm F. An improved technique for characterizing the fracture toughness via scratch test experiments. Wear 2014;313(1–2):117–24. https://doi.org/10.1016/j.wear.2014.02.015.
[121] Hubler MH, Ulm FJ. Size-effect law for scratch tests of axisymmetric shape. J Eng Mech 2016;142(12):04016094.
[122] Akono A, Ulm F, Bažant ZP. Discussion: Strength-to-fracture scaling in scratching. Eng Fract Mech 2014;119:21–8. https://doi.org/10.1016/j.engfracmech.2014.02.025.
[123] He X, Xu C. Determining strength and fracture toughness of rock from scratch tests. In: ISRM EUROCK. ISRM; 2015, ISRM-EUROCK.
[124] Santhanam M. Magnesium Attack of Cementitious Materials in Marine Environments. Netherlands, Dordrecht: Springer; 2013. p. 75–90.
[125] Chen JJ, Sorelli L, Vandamme M, Ulm F, Chanvillard G. A Coupled Nanoindentation/SEM-EDS Study on Low Water/Cement Ratio Portland Cement Paste: Evidence for C-S-H/Ca(OH)2 Nanocomposites. J Am Ceram Soc 2010. https://doi.org/10.1111/j.1551-2916.2009.03599.x.
[126] Karimzadeh A, Ayatollahi MR. Investigation of mechanical and tribological properties of bone cement by nano-indentation and nano-scratch experiments. Polym Test 2012;31(6):828–33. https://doi.org/10.1016/j.polymertesting.2012.06.002.
[127] Xu J, Shen W, Corr DJ, Shah SP. Effects of nanosilica on cement grain/C–S–H gel interfacial properties quantified by modulus mapping and nanoscratch. Mater Res Express 2019;6(4):45061. https://doi.org/10.1088/2053-1591/aafdbb.
[128] Hodzic A, Stachurski ZH, Kim JK. Nano-indentation of polymer–glass interfaces Part I. Experimental and mechanical analysis. Polymer 2000;41(18):6895–905. https://doi.org/10.1016/S0032-3861(99)00890-3.
[129] Habelitz S, Marshall SJ, Marshall GW, Balooch M. The Functional Width of the Dentino-Enamel Junction Determined by AFM-Based Nanoscratching. J Struct Biol 2001;135(3):294–301. https://doi.org/10.1006/jsbi.2001.4409.
[130] Hu C, Li Z. A review on the mechanical properties of cement-based materials measured by nanoindentation. Constr Build Mater 2015;90:80–90. https://doi.org/10.1016/j.conbuildmat.2015.05.008.
[131] Shu C, Qiao P. Characterization of Microscopic Interface of Concrete by Nano-Scratch Tests. Chinese Quarterly of Mechanics 2015;36(02):205–12 (in Chinese).
[132] Königsberger M, Pichler B, Hellmich C, Olek J, Olek J. Micromechanics of ITZ-Aggregate Interaction in Concrete Part II: Strength Upscaling. J Am Ceram Soc 2014;97(2):543–51. https://doi.org/10.1111/jace.12606.
[133] Königsberger M, Pichler B, Hellmich C, Olek J, Olek J. Micromechanics of ITZ-Aggregate Interaction in Concrete Part I: Stress Concentration. J Am Ceram Soc 2014;97(2):535–42. https://doi.org/10.1111/jace.12591.
[134] Ren X, Zhang L. Experimental study of interfacial transition zones between geopolymer binder and recycled aggregate. Constr Build Mater 2018;167:749–56. https://doi.org/10.1016/j.conbuildmat.2018.02.111.
[135] Zhang P, Gao Z, Wang J, Guo J, Hu S, Ling Y. Properties of fresh and hardened fly ash/slag based geopolymer concrete: A review. J Clean Prod 2020;270:122389. https://doi.org/10.1016/j.jclepro.2020.122389.
[136] Huang H, Lecampion B, Detournay E. Discrete element modeling of tool-rock interaction I: rock cutting. Int J Numer Anal Methods Geomech 2013;37(13):1913–29. https://doi.org/10.1002/nag.2113.
[137] Richard T, Dagrain F, Poyol E, Detournay E. Rock strength determination from scratch tests. Eng Geol 2012;147–148:91–100. https://doi.org/10.1016/j.enggeo.2012.07.011.

[138] Němeček J, Hrbek V. Nanoindentation Assessed Fracture Toughness of Cement Paste, Defect and Diffusion. Forum 2016;368:186–9. https://doi.org/10.4028/www.scientific.net/DDF.368.186.
[139] Yao Y, Hu C, He Y, Wang F. Measurement on Fracture Toughness of Cement-Based Materials Based on Micro-Scratch Test. Journal of the Chinese Ceramic Society. 2022;50(2):452–6. https://doi.org/10.14062/j.issn.0454-5648.20210354.
[140] Reda Taha MM, El-Dieb AS, Abd El-Wahab MA, Abdel-Hameed ME. Mechanical, Fracture, and Microstructural Investigations of Rubber Concrete. J. Mater. Civ. Eng. 2008;20(10):640–9. https://doi.org/10.1061/(ASCE)0899-1561(2008)20:10(640).